Journal of Nuclear Materials 523 (2019) 510–537

Contents lists available at ScienceDirect

Journal of Nuclear Materials

journal homepage: www.elsevier.com/locate/jnucmat

Ferritic-martensitic steels for fission and fusion applications

C. Cabet [a], F. Dalle [b], E. Gaganidze [c], J. Henry [b, *], H. Tanigawa [d]

[a] DEN-Service de Recherches de Métallurgique Physique (SRMP), CEA, Université Paris-Saclay, 91191, Gif-sur-Yvette, France
[b] DEN-Service de Recherches Métallurgiques Appliquées (SRMA), CEA, Université Paris-Saclay, 91191, Gif-sur-Yvette, France
[c] Karlsruhe Institute of Technology, Institute for Applied Materials, Hermann-von-Helmholtz-Platz 1, 76344, Eggenstein-Leopoldshafen, Germany
[d] National Institutes for Quantum and Radiological Science and Technology, Aomori, Japan

ARTICLE INFO

Article history:
Received 14 February 2019
Received in revised form
23 May 2019
Accepted 31 May 2019
Available online 3 June 2019

ABSTRACT

Compared to austenitic stainless steels, largely employed in the early fission reactors, high chromium Ferritic/Martenstic (FM) steels, developed since the first half of the 20th century for fossil-fuel power-plants, have a number of advantageous properties among which lower thermal expansion, higher thermal conductivity and better void swelling resistance. At the beginning of the 1970s, FM steels found their first nuclear application as wrapper and fuel cladding materials in sodium-cooled fast reactors. They are now the reference materials for in-vessel components of future fusion reactors, and are considered for in-pile and out-of-pile applications in Generation IV reactors as well as for various other nuclear systems. In this paper, after an introductory historical overview, the challenges associated with the use of FM steels in advanced reactors are addressed, including fabrication, joining and codification issues. The long term evolution of mechanical properties such as the creep and creep-fatigue behaviors is discussed and the degradation phenomena occurring in aggressive environments (lead alloys, high temperature gases, super-critical water and CO_2, molten salts) are detailed. The paper also provides a brief overview of the radiation effects in FM steels. The influence of the key radiation parameters e.g. temperature, dose and dose rate on the microstructure and mechanical properties are discussed. The need to better understand the synergistic effects of displacement damage and helium produced by transmutation in fusion conditions is highlighted.

Contents

* Corresponding author.
E-mail address: jean.henry@cea.fr (J. Henry).

https://doi.org/10.1016/j.jnucmat.2019.05.058
0022-3115/

1. Introduction: historical overview

1.1. Ferritic-martensitic steels for fission reactors and advanced nuclear systems

In 1959, when the Journal of Nuclear Materials was created, the first Tokamak fusion device had just began operation in Russia while commercial electricity production using nuclear fission was already a reality, albeit in some cases at small scale, with several reactors of various types in operation worldwide, such as the Vallecitos boiling water reactor and the Shippingport pressurized water reactor in the USA, gas cooled reactors (Calder Hall MAGNOX reactors in the UK, G1 and G2 UNGG reactors in France), the Obninsk liquid metal cooled fast reactor in Russia, and the on-going construction of other types of reactors, for instance the heavy water moderated Nuclear Power Demonstration (NPD) reactor in Canada [1–4]. That year, G3 gas cooled reactor started up in Marcoule France, Dresden-1, the first privately financed nuclear power plant built in the United States went critical, as well as the BR-5 sodium cooled fast reactor (Obninsk, Russia) and the Dounreay NaK cooled fast reactor (UK), that three years later became the first fast reactor in the world to supply power to the grid [5,6].

High chromium ferritic and martensitic steels (referred to as FM steels in the following), typically containing 9–12 wt% Cr, had been developed since the 1930s, first for use in the petrochemical industry, and later for gas turbines and conventional fossil fuel power plant applications [7,8], but they were not used as structural and cladding materials in the early nuclear reactors for which conventional austenitic stainless steels were largely employed. Following the discovery of the irradiation-induced void swelling phenomenon at the end of the 1960s [9], it soon appeared that swelling behavior was a key parameter for fast reactor core materials selection [10–12]. Contrary to conventional austenitic stainless steels, FM steels were found to be highly resistant to void swelling [13] and therefore during the 1970s they were selected, or envisaged, as materials for core components. The chosen steels were for instance 12Cr-1MoVW (HT9 grade) in the USA, unstabilized 9Cr-1Mo (EM10) and duplex 9Cr-2MoVNb (EM12) in France, 11Cr-MoVNbW (PNC-FMS) in Japan, 12Cr-MoVNb (FV448, 1.4914, EP-450) in the UK, Germany and in the former USSR [14–23]. These materials were used for the fabrication of fuel assemblies irradiated in various fast reactors worldwide, among which EBRII (Experimental Breeder Reactor II) and the FFTF (Fast Flux Test Facility) in the USA, Phénix and SuperPhénix in France, PFR (Prototype Fast Reactor) in the UK, BOR 60, BN 350 and BN 600 in the USSR. In most cases, these alloys were commercially available steel grades, belonging to the "first generation" of FM steels developed in the 1960–70s, whose maximum service temperature was evaluated to be around 560 °C [7,24]. Therefore, due to their limited strength and creep performance at high temperature, the selected steel grades were mostly employed for the fabrication of wrappers (or ducts), since their upper operating temperature in liquid metal cooled fast reactors did not exceed about 550 °C. However, in some cases, alloys such as 12%Cr alloys HT9, EP-450, FV448 and 9% Cr EM12 were also used for cladding. Owing in particular to their excellent dimensional stability under irradiation, the application of FM steels as core materials in fast reactors was a success. Fuel subassemblies fabricated using FM steels have reached high burnups with associated displacement doses on the steels up to about 150–160 dpa [25,26].

Due to their excellent swelling behavior and the positive operating experience of past fast reactors, FM steels have been chosen as in-core materials of recently build or planned new reactors. For instance, EP-450 is used as wrapper material in the Russian fast reactor BN-800, that was connected to the grid at the end of 2015 [27]. Various FM steels have been selected for wrappers of future Generation IV (GEN-IV) Na-cooled fast reactors [28], for example EM10 steel for the wrapper of ASTRID (Advanced Sodium Technological Reactor for Industrial Demonstration) [29] and PNC-FMS steel for JSFR (Japan Sodium-cooled Fast Reactor) [30]. FM steels are also possible candidate materials for core components of other future reactors, such as BN-1200 [31], CFR1000 (China Fast Reactor 1000) [32] and PGSFR (Prototype Generation-IV Sodium-cooled Fast Reactor) [33].

Until the 1970s, the materials used for the components of the containment system of sodium-cooled fast reactors (cold and hot leg piping, intermediate heat exchanger, reactor vessel) were predominantly austenitic stainless steels, in particular types 304 and 316. However, due in particular to their susceptibility to aqueous stress corrosion cracking in the presence of chloride and caustic contaminants, austenitic stainless steels were in most cases rejected for steam generator applications. Instead, low chromium ferritic steels such as 2.25Cr-1Mo were often selected as steam generator tubing materials [34,35]. In the UK, 9Cr-1Mo steel was successfully used in the evaporators and parts of the superheaters of the Advanced Gas Cooled Reactor (AGR) steam generators and therefore chosen as material for the replacement reheater unit for PFR following sodium leaks which had occurred in units made of 316 steel [8,36,37]. In addition, pressure tube parts of the CANDU (Canada Deuterium Uranium) reactors were made of a 12%Cr steel [38].

In the US, starting in the mid 70s, a development program of an improved, high strength, FM steel was conducted by ORNL in collaboration with industry [39,40], initially for sodium-cooled fast reactor steam generator application. It was later recognized that such a steel could be envisaged as sole material for the sodium transport system [41], thereby eliminating the difficulties associated with joining components made of austenitic and ferritic steels. The outcome of this program, in the early 1980s, was a modified 9Cr-1Mo steel with controlled additions of Nb, V, and N, which has since become known as mod. 9Cr-1Mo or grade 91/T91. Due in particular to the precipitation of a fine dispersion of V, Nb carbonitrides following normalization and tempering treatments, T91

exhibited higher creep strength than standard commercial alloys in the range 2.25Cr-1Mo to 12Cr-1Mo commercially available at the time [39]. T91 received initial ASME code approval in 1983 for boiler tubing applications [42] and was subsequently widely used in the power and petrochemical industries [42,43]. In particular, it became the choice for conventional power plants in the 90s that were designed for higher temperatures than the preceding plants (up to 590 °C) [7]. Since the allowable stresses directly determine the required thickness of material, and owing to the improved creep properties of T91 at high temperature, the replacement of low chromium steels such as 2.25Cr-1Mo lead to a significant reduction of tube thicknesses and a decrease of components weight and cost [44]. In addition, compared to austenitic stainless steels, FM steels such as T91 have a smaller thermal expansion coefficient and a better thermal conductivity, leading to lower thermally induced stresses, better thermal fatigue properties and therefore increased component lifetime.

In the nuclear power field, T91 has been envisaged for the Steam Generator of the European Fast Reactor (EFR) project in the 80s. The high fracture toughness of T91 thick products was valuable for some parts of this component. Following the EFR project, T91 has been recently considered in France as a candidate for the steam generator of the ASTRID prototype [45]. An other innovation being evaluated as part of the ASTRID project is to use a power conversion system based on the super-critical CO_2 Brayton cycle, because of its high efficiency. FM steels are possible candidate materials for this application [46].

T91 has also been chosen to fabricate the steam generator in the Prototype Fast Breeder Reactor (PFBR), under construction in Kalpakkam [47], and was selected to build the steam generators of future Commercial Fast Breeder Reactors (CFBR) in India. Finally, T91 was chosen as structural material for the primary and secondary heat transport system components (piping, intermediate heat exchanger and steam generator) of JSFR [48,49]. Because of its good thermomechanical properties already highlighted above, the use of T91 allowed to design primary and secondary piping layouts with drastically shorter length and fewer elbows as compared to a conventional design using piping made of austenitic stainless steel.

In addition to sodium-cooled fast reactors, there has been a renewed interest since the beginning of the 21st century for nuclear power plants cooled with lead alloys. For instance, the Lead-cooled reactor (LFR) is one of the Generation IV systems [50]. Liquid Lead or liquid Lead-Bismuth eutectic (LBE) were also chosen as coolant for several concepts of Accelerator Driven Systems (ADS). ADS are subcritical nuclear systems developed for different applications, in particular the transmutation of nuclear waste [51,52]. They consist of a high power neutron source (the spallation target) used to drive a subcritical core. FM steels have been selected, or envisaged as possible candidate materials for structural and core materials of various LFR and ADS concepts. The proton beam window of the MEGAPIE (MEGAwatt Pilot Experiment) LBE spallation target, the first liquid metal target successfully operated at a power close to 1 MW, was made of T91 [53,54]. T91 was also considered as wrapper and possibly cladding material for the lead-cooled ELFR (European Lead Fast Reactor) and ALFRED (Advanced Lead Fast Reactor European Demonstrator, a smaller size LFR demonstrator) [55–57] as well as for the wrapper, core support plate and spallation target window of MYRHHA (Multi-purpose hYbrid Research Reactor for High-tech Applications), an accelerator-driven LBE cooled system designed to operate both in subcritical and critical modes [58,59]. EP-850, a 12%Cr FM steel with high Si content (1–1.3%) developed in Russia for increased resistance to corrosion effects in lead, is the prime candidate material for the fuel assemblies, including fuel cladding, of the planned lead-cooled reactor BREST-OD-300 [27,60].

Indeed, the effect of aggressive coolants such as lead alloys on the performance of FM steels is a key issue, addressed in the section about environmental effects. FM steels have been found to be globally more sensitive to corrosion, erosion and Liquid Metal Embrittlement (LME) in lead alloys compared for instance to 316 stainless steels [61]. Mitigation strategies, for instance using dedicated coatings [62], are to be developed to control the possible degradation of the mechanical properties due to the liquid metal. Synergistic effects between irradiation and LME have also recently been evidenced in the case of FM steels. Hardening of FM steels induced by irradiation at low temperature was shown to enhance LME effects [63]. This issue is particularly important in the case of systems cooled with LBE such as MYRHHA, which will operate at lower temperatures than reactors cooled with liquid lead.

Concerning the gas-cooled GEN IV systems, a 9Cr FM steel such as T91 is a candidate material for the hot reactor vessel [64], which should operate at temperatures close to about 450 °C if no separate cooling circuit is included in the reactor design. So far, no reactor vessel using 9Cr FM steels has ever been built. This will require the fabrication of thick 9Cr FM steel products with good control of the microstructure and the mechanical properties throughout the thickness. Joining of high-thickness components made of 9Cr FM steels is also an important technological challenge, as well as the evaluation of the long term thermal ageing effects.

FM steels were also evaluated as possible candidate materials for supercritical water reactors (SCWR). Most of the investigated FM steels were found to have better stress corrosion cracking resistance in SCW than other classes of metallic alloys, however due to their poorer corrosion behavior, they are probably less suitable for use in a SCW environment [65,66].

Finally FM steels such as HT9 are foreseen to be used as wrapper and cladding materials for the Travelling Wave Reactor (TWR), a sodium cooled “breed and burn” fast reactor concept, whose development started a few years ago [67]. While in the case of GEN IV concepts, for instance SFR, the fuel cladding material would need to withstand up to 200 dpa to meet the fourth generation requirements, in the case of the TWR, peak damage dose on the cladding is expected to reach 600 dpa, a value far beyond the maximum irradiation dose ever achieved in a neutron irradiated FM steel. This push towards very high damage levels in revolutionary nuclear systems has sparked in recent years numerous irradiation experiments of FM steels to several hundreds of dpa using ion beams, with the aim to investigate the microstructural evolutions occurring at very high damage doses, in terms of swelling, intergranular segregation and precipitation behaviors [68–72].

1.2. FM steels for fusion reactors

As in the case of the fission reactors, FM steels were not initially considered as possible structural materials for fusion reactors. The early candidate materials for first wall and breeding blanket applications were for instance austenitic stainless steels, Ni-based superalloys, Ti alloys, and refractory metals (V, Nb, Mo) and their alloys [73–77]. FM steels were not originally envisaged for fusion applications in particular due to concerns about the use of ferromagnetic materials in an environment with high magnetic fields, because of magnetostatic forces on ferromagnetic components and also possible effects on plasma control as a result of magnetic field perturbations. However, early assessments confirmed by more recent studies have shown that the complications associated with the presence of ferromagnetic materials can be managed but have to be taken into account in the reactor design [78–81]. FM were envisaged as alternative structural materials for fusion reactors at the end of the 1970s, when the first results of irradiation campaigns

on FM steels performed as part of the fast reactor programs in Europe and the USA were becoming available [82,83]. As already emphasized above, in addition to their high swelling resistance compared to austenitic stainless steels, the FM steels also have better thermal stress resistance, and therefore less prone to thermal fatigue problems in fusion reactors operating in pulse mode.

The need to assess the effects on the properties of FM steels of the high quantities of transmutations products, in particular helium and hydrogen, generated in a fusion environment was recognized very early by the fusion materials scientists. In the absence of an intense 14 MeV neutron source, different methods were used to simulate fusion irradiation conditions, such as Ni doping as well as single and multiple ion beam irradiations [84–86]. For instance tensile tests after helium implantation as well as in-beam creep tests [87,88] showed the high resistance of FM to the elevated temperature helium embrittlement phenomenon, in contrast to austenitic stainless steels. Indications of this resistance had already been provided at the end of the 1960s, for instance through the work of Böhm and Hauck, whose findings were published in the Journal of Nuclear Materials [89,90]. To our knowledge, these articles were the first ones relative to FM steels ever published in this Journal.

However, it was later found that FM steels are by no means immune to He-induced effects. Indeed, based in particular on tests performed on specimens irradiated in spallation conditions or implanted with He, it was concluded that helium concentrations above about 500 appm, especially when generated at low temperatures (typically below 400 °C), enhance irradiation-induced embrittlement of FM steels, with the occurrence of intergranular fracture mode with increasing helium content and irradiation dose [91,92]. This may substantially limit the lifetime of fusion components especially for water-cooled concepts of fusion reactors. The helium contents tolerable in the structural materials of fusion reactors still remain to be determined by using future Fusion Neutron Source (FNS) facilities.

The FM steels evaluated for fusion applications were firstly those selected as part of the fast reactor programs. Specific fusion related steel development programs were then initiated, as for instance in Europe, where the “MANET” steel (Martensitic steel for the Next European Torus) was the result of the optimization of FV448/1.4914 commercial alloys, with in particular improved creep, impact and toughness properties [93,94]. Furthermore, because the irradiated structural materials of the breeding blankets are the major source of long-term radioactivity in a fusion reactor, it was early recognized that, in view of the public acceptance of fusion hailed as a “clean” energy source in contrast to fission, low (or reduced) activation steels should be developed [95,96]. Following an appropriate cooling time after reactor shut-down, this could allow simplified waste management like shallow land burial or possibly even material recycling. To reach this goal, activation calculations showed that important alloying elements in conventional FM steels like Nb and Mo with long decay times after irradiation must be replaced by metallurgically equivalent Ta and W [97–99]. Likewise, the concentrations of Ni, Cu, Al, Co and various impurity elements with high long-term radioactivity must be drastically reduced. From the mid-1980s onwards, several experimental reduced activation FM (RAFM) steels were designed in the USA, Europe and Japan [94,100–109]. In order to accelerate the development of RAFM steels, an international collaboration was set-up in 1992 within the framework of the International Energy Agency (IEA). As part of this collaboration, two 5-ton heats of F82H, a Japanese 8Cr2WVTa RAFM steel [102], were produced with a commercial vacuum induction furnace using high-purity raw materials [110,111]. A few years later, a total of 11 tons of EUROFER97, the 9Cr1WVTa reference RAFM steel in Europe since 1997, were fabricated by clean steel making technologies using carefully selected raw materials [112]. Gamma dose rate calculations based on the measured chemical compositions of the industrially produced F82H and EUROFER97 heats showed that after irradiation with fusion neutrons to an integrated first wall loading of 12.5 MWy/m^2, both materials could be stored as low-level waste after 100 years [113]. The dose rates values for F82H were however found to be up to one order of magnitude lower than in the case of EUROFER97, mainly due to a lower residual Nb concentration. Further progress towards the ultimate goal to meet the “hands-on” dose rate target after 100 years seems to be technically feasible, but will require the use of advanced steel making technologies, high purity raw materials as well as dedicated production tools reserved for RAFM steels, so as to avoid impurity pick-up during fabrication [113,114].

Since 2002, China Low Activation Martensitic (CLAM) steel, a 9Cr1.5WVTa alloy, is being developed [115,116]. The first large scale (4.5-ton) CLAM steel batch was produced in 2011. Other countries, notably India, Korea and Russia, have also started developing their own variants of RAFM steels [117–121]. It should be noted that EK-181 (also known as RUSFER), a 12Cr2WVTaB RAFM steel developed in Russia, is envisaged for fusion as well as fission applications in sodium cooled fast reactors [27,31,121]. F82H and EUROFER97 have currently the largest data base, including data after fast neutron irradiation up to 70 dpa (see below the section on irradiation effects) [122–124]. Both steels have been produced in various product forms, and design code qualification is in progress: for instance EUROFER97 was recently introduced (under probationary status) in the French nuclear components design and construction code RCC-MRx [125,126].

The mechanical performance at high temperature of current RAFM steels, for instance in terms of thermal creep behavior, is comparable to that of “second generation” FM steels such as T91 [127]. In order to achieve better thermodynamic efficiency, it would be desirable to increase the maximum operating temperature of the structural steels. The use in fusion reactors of the most advanced conventional FM steels with very high creep resistance is not possible because these steels contain radiologically undesired elements such as Co [128]. Therefore, new RAFM steels are being developed since a few years with the objective to achieve superior high temperature mechanical properties, and possibly better behavior under irradiation. The followed approaches include applying thermomechanical treatments (TMT) and the optimization of the chemical compositions guided by the use of computational thermodynamics [129–134].

In the following, we will focus on the current knowledge regarding the performance of FM steels as materials both for in-pile and out-of-pile nuclear applications. The present article does not intend to provide a comprehensive overview. For instance, the metallurgy of FM steels will not be addressed and the reader is referred to the excellent monograph on FM steels by Klueh and Harries [135]. We will concentrate on some specific important issues, beginning with fabrication and joining. As some reactor designs foresee very long operating lifetimes, FM steels behavior under long-term thermomechanical solicitations will be reviewed, in terms of creep and creep-fatigue resistance as well as thermal aging effects. Code qualification issues will also be briefly addressed. Radiation effects in fission and fusion environments on the microstructural evolution and on the mechanical properties of both conventional and Reduced Activation FM steels will be described with emphasis on swelling behavior and irradiation creep, and on the evolution of tensile and impact properties under irradiation. Examples of environmental degradations and associated mitigation measures, a key issue for the performance of materials in particular when in contact with aggressive coolants at

high temperatures, will be described in some detail.

2. Fabrication and joining

Many nuclear components for fission and fusion applications are typical assemblies of plates, grids, shells and tubes with a certain amount of machining. Commercial FM alloys are currently produced in various shapes at an industrial level, mainly for conventional power and petrochemical industries. In order to fulfill nuclear requirements, it is necessary to demonstrate the technical capability of steelmakers and manufacturers to meet new designs, code and licensing requirements, as well as specific material performances. For fission and fusion applications, it is also necessary to address joining issues, sometimes using state-of-the-art technologies. Illustrations of these challenges and examples of on-going activities are given below.

2.1. Specific product forms and manufacturing processes

The production of FM heats usually implies vacuum arc or induction melting, and purification through vacuum arc re-melting, to produce chemically and mechanically homogeneous ingots. Development aspects mainly focus on large-scale smelting and purification techniques. For RAFM steels in particular, there is a need to reduce neutron-induced activation and to lower impurities levels [116]. In addition, the latest Gen. IV designs include some product forms like seamless cylindrical shells with large diameters, thin heat transfer tubes and thick forgings for the tubesheets of Steam Generators (SG) [45,136]. Several industrial fabrication routes are possible to produce such products: open die forging, (ring) rolling, extrusion … as long as the hot working rate is sufficient. The availability of large-scale production capabilities of the sizes required for present designs needs to be guaranteed. In the 90s, the feasibility of producing heavy products (plates or forgings) in grade 91 for pressure vessels with a thickness up to 300 mm was demonstrated [137]. More recently, the steelmaker Industeel (Arcelormittal Group), whose experience is large for thin plates devoted to the pipe industry, renewed the industrial feasibility of thick plates (140 and 210 mm), which were shown to be chemically and mechanically homogeneous, according to the Gen. IV nuclear requirements [138].

For the production of steam generators, the industrial capacity to produce tubes as long as possible is also looked for, in order to limit the number of weldments and to ensure an enhanced reliability against sodium-water reaction. The Vallourec group produces a wide size range of hot finished seamless tubes in accordance with grade 91 standards [139]. The maximum length of the tubes dedicated to SG application is stated to be 25 m, which corresponds to the required length of the straight tube SG concept for the French ASTRID reactor [45]. The possibility to supply longer tubes depends on both the investment capacity of the manufacturer and the transport issue. In that respect, T91 has been selected by the Indira Gandhi Centre for Atomic Research (IGCAR) to constitute the Steam Generator in the Prototype Fast Breeder Reactor (PFBR), with a tube length of 23 m [47]. Furthermore the Indian nuclear community plans to build a Steam Generator with a length of 30 m for future Commercial Fast Breeder Reactors (CFBR), also using T91.

Note that, since T91 steel is less ductile than, for instance, austenitic steels, the bowing process of tubes presents some difficulties, especially during cold bending of a material procured at high hardness [42]. Some design solutions may be found to make up for the limited formability of this steel. Otherwise the bending equipment needs to be adapted to hard materials, using for example computer-aided induction machines [139] or machines equipped with back axial thrust [140]. The post-bending heat treatment rules, sometimes necessary to relieve excessive stresses or to prevent detrimental effects of recovery or recrystallization, are not well defined and represent an area for further research.

In the end, the manufacturing process has a strong influence on the mechanical performances of the specific products, since it may affect several metallurgical features: grain size and shape, precipitation processes, segregations … Apart from demonstrating the industrial capacity to produce component parts, the other aim is to check that their properties are not too far from the existing mean values, coming from databases obtained on smaller sheets or tubes. This is the case in Ref. [138] or [142], where the variation of tube or forging thicknesses is negligible on tensile and creep properties. The mechanical performances of FM steels are also largely dependent on the final heat treatment conditions. The typical industrial treatments applied to these steels imply successive normalization/quenching/tempering steps. An example taken as a guide for the industrial practice is given in Ref. [139]. Fig. 1 shows the extent of grade 91 mechanical properties after tempering at different temperatures between 650 and 850 °C. With an increase of tempering temperature up to A_{c1}, the yield strength, tensile strength and hardness decrease whereas the impact toughness increases. Tempering above A_{c1} results in opposite trends due to the formation of as-quenched martensite. As to the heat treatment durations, they usually vary with the product form. They increase with the thickness of the product, so that the core temperature reaches the required level. Adequate temperature monitoring is recommended during the whole process, since T91 steel is less temperature-tolerant than its low-allied precursors. Regarding RAFM steels, heat treatment specification and acceptance values are similar to those of conventional FM steels, at least in the case of the most mature ones, F82H and EUROFER97 [125].

2.2. Weldability

Successful welding generally implies defect-free weldments, optimal microstructural features and basic mechanical properties

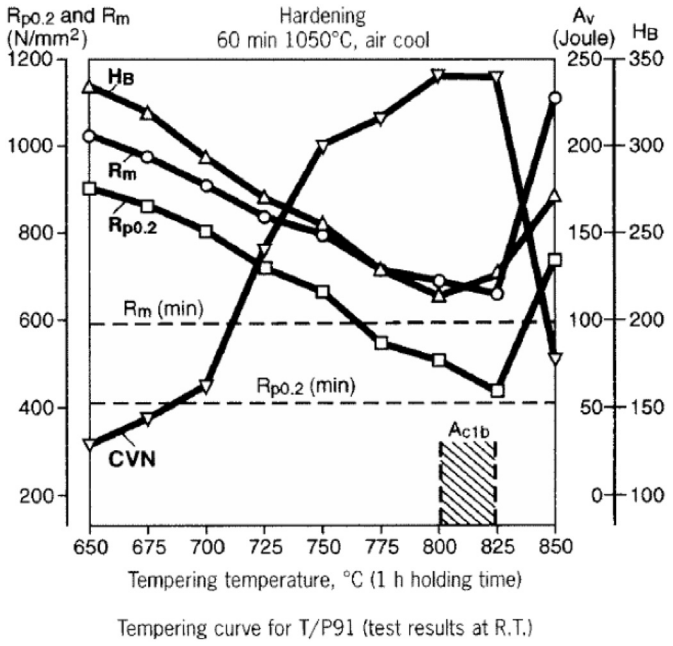

Fig. 1. Variations of $R_{p0.2\%}$, R_m, HB hardness and CVN toughness for T91 as a function of tempering temperature (test results at room temperature) [139].

as close as possible to those of the base metal. The high sensitiveness of FM steels in the field of weldability is one of their main characteristic features, since some procedures are to be followed cautiously to obtain good quality weldments. Many failures in conventional power plants were historically due to faulty heat treatments that resulted from the lack of training and supervision [143]. However, positive feedback confirm that these steels can be joined by several arc-welding processes and by manual and automatic techniques, like shielded metal arc welding (SMAW), gas tungsten arc welding (GTAW), gas metal arc welding (GMAW) or submerged arc welding (SAW). Although a slow process, GTAW is reported to produce the highest quality welds [143]. Advanced, low-heat input and high-speed processes such as electron beam (EB) and laser welding are also being developed and used on an increasing scale since the 80s [144], notably for the dissimilar welding of FM and austenitic steels [145] or for the development of RAFM steels joining for fusion applications [146,147].

Several lever effects are used to achieve good quality weldments: the optimization of welding procedure and parameters, the development of appropriate filler metal and the application of a Post-Weld Heat Treatment (PWHT). For example, to prevent cold cracking to which T91 has been proven to be sensitive, the pre-heat, interpass and post-heat temperatures are to be controlled during the welding process. Preheating is usually carried out at about 200 °C, allowing hydrogen to diffuse out of the weld zone. The joining of T91 also requires low hydrogen welding products [137]. In this way, during the final cooling step, the martensitic transformation takes place under low stress and low embrittlement risks. The optimization of filler metal composition is indeed a significant area of development, either to limit hot cracking sensitivity of FM steels, or to obtain satisfactory properties of welded joint (Heat Affected Zone and weld metal). The chemical composition of weld metal has consequences on the delta ferrite content, interfacial segregations, liquation phenomena … Commercial filler products for grade 91 have mainly been optimized for creep resistance in the frame of conventional power applications, and not for toughness, which is a great concern in irradiation environments. Thus one of the criteria for a nuclear weld metal chemical composition is adequate impact properties. For example, the French regulation about Nuclear Pressure Equipments requires a minimal impact energy value of 60 J for base and weld metals, which industrial filler materials fail to satisfy, so that a specific optimized filler material for grade 91 had to be developed [45]. As to RAFM steels, in parallel to the adjustment of base metal composition, international studies are also concerned with optimizing welding parameters or filler metal chemistries, taking into account the low-activation requirements [147–149].

Following the welding operations, a high temperature PWHT is usually necessary for high chromium steels. This helps to soften the brittle as-quenched martensite of the weld metal and to reinforce the Heat Affected Zone with hardening precipitates, in order to achieve similar mechanical characteristics to those of the base metal. The necessity of PWHT is one of the main drawbacks of high chromium FM steels use, representing an economic and technical issue, absent in the case of lower chromium steels for example. There is a narrow gap between the PWHT and the tempering treatment carried out at 750–780 °C, and this high temperature operation on large and multi-shaped components gets complicated due to the required accuracy of the temperature control. An example is given by Ref. [150] with the complex manufacturing process of a wrapper tube for Japanese advanced fast reactors. The different steps imply: dissimilar GTAW welding of SUS316 tubes at each end of a 11Cr FM tube, cold drawing to produce a hexagonal tube, normalizing and tempering of the whole assembly, straightening by a hydraulic press (because of the differential thermal expansion of both materials).

When possible, hardness profiles through the welded joints are carried out to assess the PWHT efficiency. A low hardness area in the HAZ adjacent to the base steel is a characteristic feature of FM steels, at least for standard welding processes. This area corresponds to an additional tempering of the tempered martensitic structure, usually showing larger sub-grains, lower dislocation densities and larger spherical carbide particles. High energy welding methods like laser beam welding and electron beam welding imply low heat input and show extremely narrow HAZs, as can be seen on Fig. 2 taken from Ref. [151]. This figure presents the cross section images of both GTAW and EB welded F82H plates, after a PWHT at 720 °C for 1 h. The hardness profiles across each weldment show almost no softening in HAZ. Thus, depending on the welding process, a wide range of microstructures may appear in the weld metal and the heterogeneous HAZ, which has a significant effect on the overall mechanical properties. It is important to check the toughness of the weldment, as well as the possibility of type IV cracking in service conditions. This type of cracking, named after its location in the HAZ, occurs during creep solicitation, and it seems to be associated with the softest area in the HAZ. David and coworkers [143] give a valuable overview of the on-going studies dedicated to understanding these premature failures, finding their precise location and improving the type IV cracking resistance of FM steels. For codification purposes on the other hand, studies have also been dedicated to providing appropriate welded joint strength reduction factors taking into account this phenomenon [136].

The international effort about the fabrication of Breeding Blankets (BB) should finally be mentioned, as it relies on state-of-the-art welding technologies applied to RAFM grades. The BB designs and the Test Blanket Modules (TBM) consists of complex multi-layer components which include many welded structures with different thicknesses. Some manufacturing scenarios imply solid state bonding processes such as Hot Isostatic Pressing and Diffusion welding, associated with GTAW, laser or electron beam welding [116,152,153]. And beyond the welding processes, a number of issues are heightened by the complex geometries: accessibility of the welding tools, distortion induced by the welding operations, PWHT, Non Destructive Examination, reparation procedures and welding procedures qualification [154].

3. Behavior under long term thermo-mechanical solicitations

Owing to the wide variety of thermomechanical loadings and environmental conditions in a nuclear power plant, and to the life durations expected from the reactor design, the material degradation processes need to be thoroughly understood and controlled. Creep and creep-fatigue resistance, thermal aging, irradiation damage and corrosion are among the main issues that must be considered and evaluated. This paragraph addresses first the thermo-mechanical solicitations, while irradiation damage and corrosion are dealt with in the next parts of this paper. The long time performances of a material are strongly related to its microstructural stability. Therefore, many studies address the evaluation of the effects of thermal aging, creep, creep-fatigue in terms of both evolution of mechanical properties and metallurgical changes. This is illustrated in the following paragraphs.

3.1. Creep resistance

The microstructure of FM steels includes various boundaries such as prior-austenitic grain (PAG) boundaries, martensite packet, block, and lath boundaries. The high dislocation density induced by the martensitic transformation decreases during the subsequent tempering treatment, allowing to obtain a good balance between

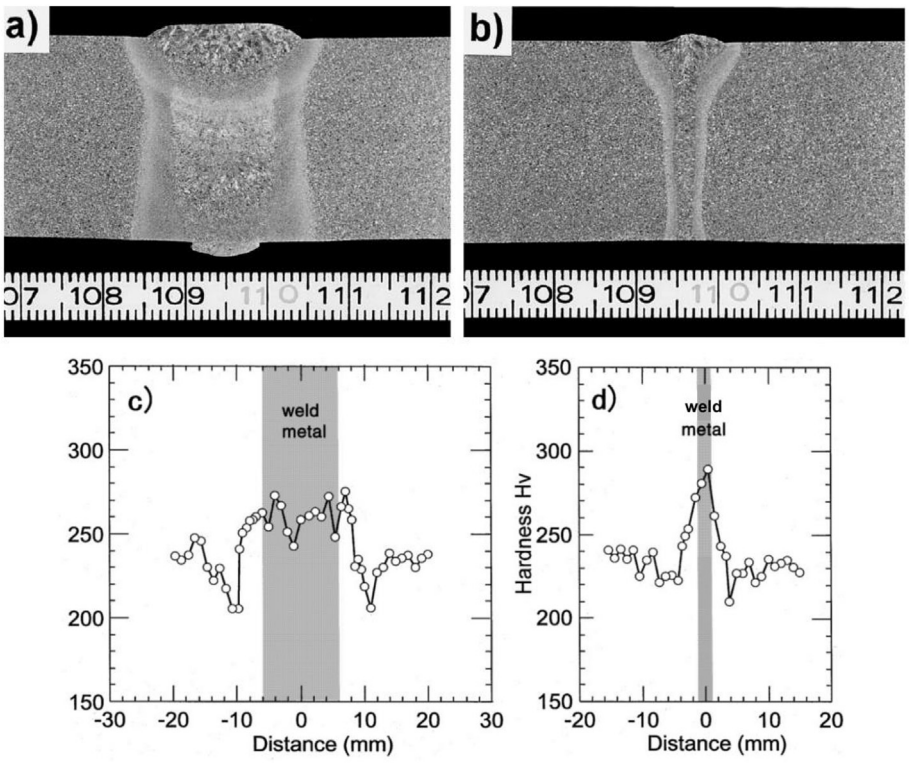

Fig. 2. Cross sections of GTAW (a) and Electron Beam (b) welded F82H plates, and corresponding hardness profiles [151].

strength and toughness of the material. The major precipitates are $M_{23}C_6$ (M: Cr, W, Mn, Mo) carbides and MX (M: Ta, Nb, V; X: N, C) carbonitrides.

FM creep-resistant steels present several strengthening mechanisms such as solute hardening, mainly attributed to molybdenum and/or tungsten, precipitation hardening by carbides, carbonitrides, dislocation and sub-boundary hardening thanks to the tempered martensitic microstructure. An enhanced creep resistance is obtained by the stabilization of the subgrain structure by the $M_{23}C_6$ carbides, mainly located on boundaries. One of the main challenges is to maintain this stability for long times at high temperatures. Indeed with time at elevated temperature (in a creep test or during service), coarsening of the $M_{23}C_6$ particles reduces their pinning effect and destabilizes the subgrain structure. Similarly, coarsening of MX precipitates reduces their strengthening effect, although MX coarsening does not occur as rapidly as for $M_{23}C_6$. In addition, Laves phase [Fe_2(Mo,W)] may form, depending on the steel composition, which removes molybdenum and tungsten from solution and reduces their hardening effect. The precipitation of a complex carbo-nitride (Z-phase [Cr(V,Nb)N]) is also reported in T91 subjected to long creep tests (more than 12000 h at 600 °C). The formation of this phase consumes MX carbonitrides and is therefore detrimental for creep resistance [155].

There is a wide area of research dedicated both to the increase of initial strengthening mechanisms with the hope of keeping a certain level of resistance at longer times, and/or to the long-term impediment of the coarsening and recovery processes. For example, the addition of boron has been reported to stabilize $M_{23}C_6$ particles, thus decreasing the rate of coarsening at elevated temperatures and ultimately stabilizing the subgrain structure [156,157]. Several groups are also designing RAFM steels with modified chemical compositions using computational thermodynamics, in order to enlarge the operating temperature window towards higher temperatures. The pursued strategies involve for instance increasing the amount of fine MX-type carbonitrides that are more resistant to coarsening as compared to $M_{23}C_6$ carbides, and therefore more efficient to pin interface boundaries during creep. Experimental RAFM steels designed along these principles have shown noticeably enhanced high temperature strength and creep properties compared to current RAFM steels, combined with good impact behavior [131,134].

Another approach may be the optimization of non-standard thermal and thermo-mechanical treatments (TMT) during FM steels fabrication. These treatments usually include an austenitization step at temperatures higher than standard practice, in order to achieve better solution annealing of precipitates, while avoiding excessive austenite grain growth. The thermomechanical processing may for instance include a hot working step in the metastable austenite range (ausforming) as well as a cold working step between the austenitization and tempering treatments. The aim of such treatments is both to refine the grain microstructure and to create an increased density of nucleation sites for small hardening precipitates. This approach has been successfully applied in both conventional and RAFM steels which exhibited improved strength and creep properties following appropriate TMT [129,130,158–160]. It should be noted however that the beneficial effects of TMT may be lost as a result of welding operations, and that some of these treatments involve tempering at relatively low temperatures, which may be unsuitable with the general practice of post-weld heat treatment. Furthermore, like in the case of conventionally processed FM steels, a cyclic softening effect also occurs in a TMT FM steel studied by Hollner et al. [161]. Finally some studies deal with the optimization of both non-standard thermo-mechanical treatments and new alloy composition, in order to produce the most favorable microstructure and precipitation state for elevated temperature strength [132,162]. Fig. 3a, taken from Zinkle et al. [127], shows creep rupture strength results of various FM and RAFM steels at 650 °C, among which new grades

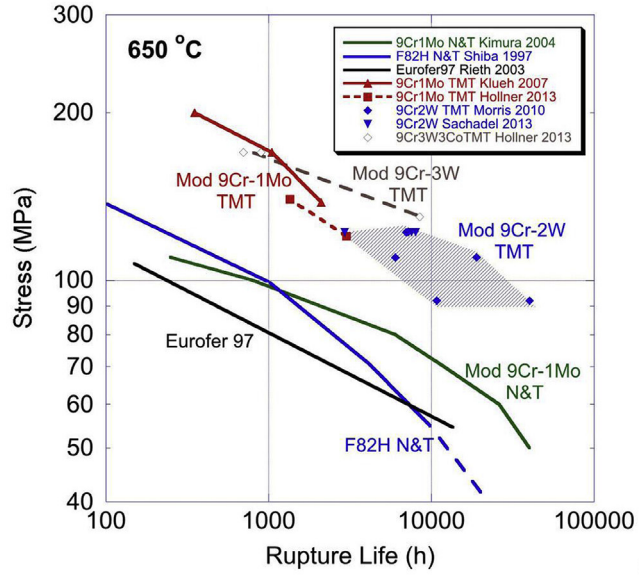

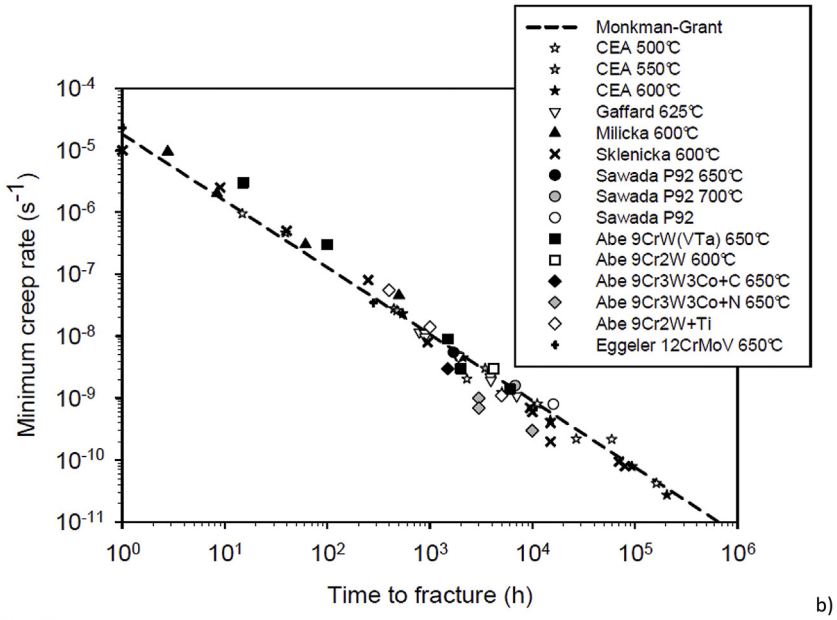

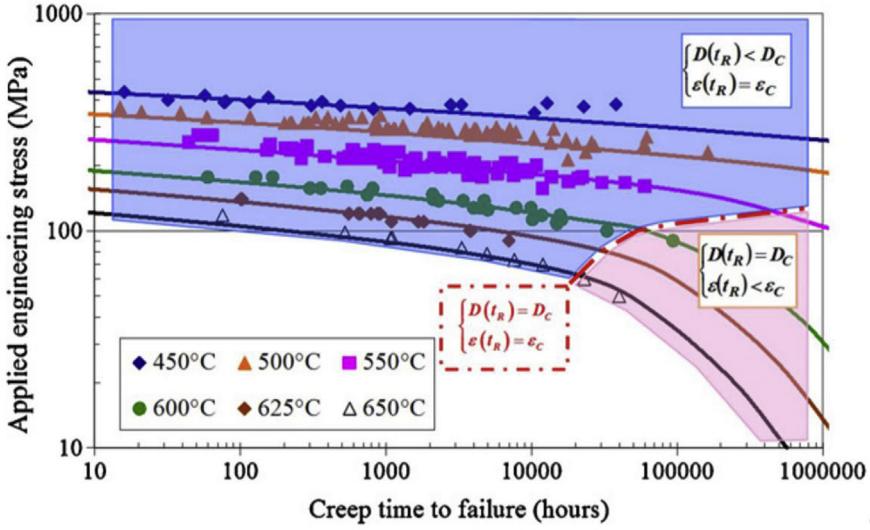

Fig. 3. Creep rupture strength of FM and RAFM steels at 650 °C, including new alloys with optimized compositions and TMT conditions [127] (a), Monkman-Grant curve for different temperatures, applied stress and chemical compositions [163] (b), Simulated (lines) and experimental (symbols) creep time-to-rupture for T91 steel (ε stands for the total calculated strain and D for the damage) [164] (c).

with both optimized chemical compositions and TMT conditions. The Mod. 9Cr-2W TMT grades are the most interesting ones since Mod. 9Cr-3W TMT contains cobalt and cannot be envisaged for reduced activation fusion applications. A significant improvement in mid-term creep rupture lifetime is achieved for these grades where MX and M_2X precipitation is promoted.

Long-term creep data are the key point for many applications, in order to help the design of structural components that may not be replaced through the lifetime of the nuclear reactor. Some long-term data or experimentally-based trend curves are publicly available for many conventional martensitic steels, thanks to academic [165,166] or prescriptive studies [167], in the framework of national or international collaborations [168,169]. As to RAFM steels, several references confirm that the creep rupture properties of F82H and EUROFER97 are comparable - or slightly inferior - to those of T91, as shown in Fig. 3a [122,125,127].

Together with the need of long-term data, the development of models and the prediction of long-term creep properties of FM steels are also topics of interest. Lim et al. have proven the Monkman-Grant relationship (linear relationship between the logarithm of the time to rupture and the logarithm of the minimum creep rate) to hold for large ranges of temperature, applied stresses and chemical compositions (Fig. 3b) [163]. Several studies discuss nevertheless an increase in the slope of the stress versus time to fracture with decreasing stress due to a loss of creep strength, which may lead to overestimate the lifetimes in service [165,166]. A change of the dominant deformation and/or damage mechanisms depending on the stress level is probably involved in this phenomenon. Massé et al. use a strain rate viscoplastic model including the effect of damage to produce numerical calculations and predictions of the creep strength of T91 (Fig. 3c) [164]. Although such an approach involves a large set of parameters, the drop-off in time-to-rupture in the creep rupture curves is well predicted over the stress and temperature ranges, and the change of failure mechanism from viscoplasticity-assisted ductile rupture to diffusion-assisted creep cavitation damage is taken into account. The improvement of such micro-mechanical models still need to be carried on, with for example, the integration of microstructural stability at long times to ensure that extrapolation is relevant.

3.2. Creep-fatigue resistance

In the case where thermal cycling is the dominant type of loading, fatigue and creep-fatigue interaction should be the most important failure modes to be prevented in the structural materials. Yet by contrast with the creep situation, the literature about cyclic tests on FM steels is less abundant. Similarly to the creep situation, material softening occurs during cyclic loading of conventional and RAFM steels, with or without holding times [170–173]. During pure fatigue or creep-fatigue tests, the stress amplitudes decrease with increasing number of cycles for all imposed amplitudes of deformation, and this phenomenon is common to a wide variety of FM steels and a large range of temperatures. In Fig. 4a, this drop represents between 30 and 40% of the stress amplitude measured during the first cycle, for a total strain amplitude $\Delta\varepsilon_t = 0.7\%$ and a temperature equal to 550 °C [174].

The microstructural modifications observed after cyclic loadings are rather similar to those observed after creep, mainly subgrain growth and dislocation density decrease [171]. The cyclic softening effect is also enhanced by a high temperature and a low strain rate, which corresponds to conditions close to those of creep tests [174]. Nevertheless the precipitation evolution, growth of existing precipitates or formation of new phases, can usually be neglected during short term creep-fatigue tests in laboratory. The softening phenomenon is mainly due to viscoplastic deformation and related

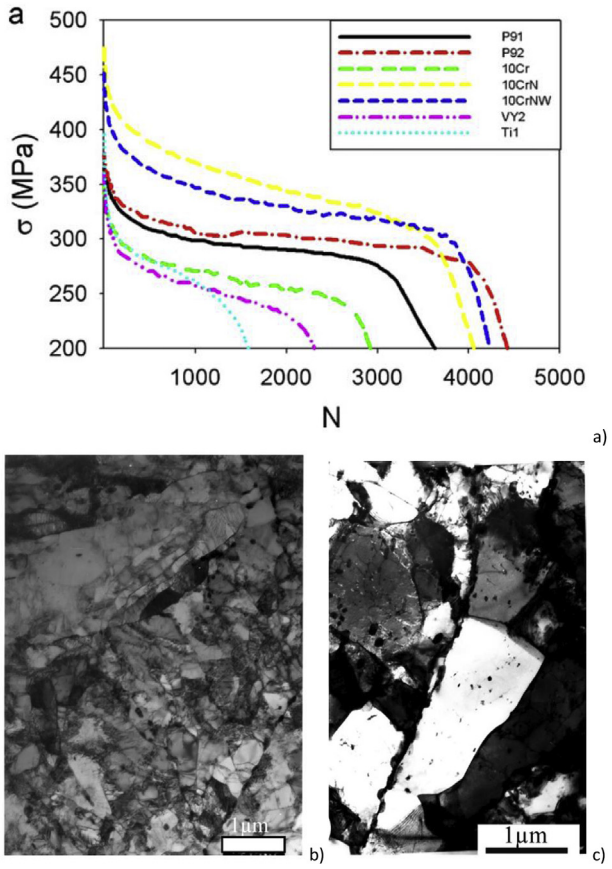

Fig. 4. Cyclic softening effect of various FM steels under pure fatigue loading ($\Delta\varepsilon_t = 0.7\%$, T = 550 °C) in terms of maximum stress per cycle versus number of cycles (a), TEM observation of T91 microstructure in the as-received condition (b) and after creep-fatigue test (550 °C, $\Delta\varepsilon_{fat.} = 0.7\%$, $\varepsilon_{creep} = 0.5\%$) (c) [174].

dislocations glide and climb. Sauzay et al. proposed a microstructural mechanism based on the disappearance of low-angle boundaries made of dislocation networks, annihilated by mobile dislocations during viscoplastic deformation [175]. TEM observations of cycled T91 are reported in Fig. 4 showing the subgrain growth following a creep-fatigue test with $\Delta\varepsilon_{fat.} = 0.7\%$ and $\varepsilon_{creep} = 0.5\%$. Some isolated precipitates are observed after cycling, probably meaning that the dislocations of the corresponding low angle boundaries have vanished despite the pinning effect of these pre-existing precipitates. Similar changes in microstructure are reported by Ref. [173] in cycled Eurofer 97 at 550 °C.

The microstructural modifications occurring during cyclic loading can lead to a drastic deterioration of the creep strength. Depending on the tests conditions, the minimum creep rate of T91 after cyclic loading can be more than 100 times faster than in the as-received state [174]. Environmental effects may also occur, acting in synergy with softening or damage mechanisms: it has been reported that the softening is more important in air than under vacuum [176] and that holding times in compression are more damaging than holding times in tension due to the rupture of the oxide layer after the compression step [170]. All this may lead to maximum allowable stresses much smaller than the limits implemented in the current design rules.

3.3. Microstructural stability during long-term thermal exposure

Many studies aim at evaluating the effects of thermal ageing on 9–12%Cr steels. Typical thermal ageing experiments have been

performed at temperatures ranging between 400 and 650 °C, for ageing durations up to 100000 h [139,177,178]. Ageing experiments at higher temperatures (700–800 °C) are reported by Ref. [179] for wrapper and cladding applications in Japanese JSFR. Time-temperature equivalences could be interesting to avoid long-term experiments by increasing the testing temperature, but it must be guaranteed that the temperature increase does not change drastically the microstructural evolutions. For fission applications, an important concern is the assessment of aged material properties (tensile, impact, short-term creep strength to rupture) to prevent brutal failure after a long period of service [45]. This may lead to the definition of ageing reduction factors in design codes. Asayama gives the example of the tensile strength reduction factor of T91 after 300 000 h at 550 °C, equal to 0.89 in the ASME code [136]. For fusion applications, embrittlement under irradiation is reported at high temperatures where no irradiation-induced hardening occurs in RAFM steels, but where significant thermal ageing coupled with irradiation-enhanced precipitation is reported [181].

Literature studies usually show that the tensile properties after thermal ageing hold for a certain domain of time-temperature, whereas the impact properties are more prone to degradation [142,182]. This is the case of Tanigawa et al. [182] reporting a limited decrease of F82H yield stress after 100000 h up to 550 °C (Fig. 5a), together with a substantial DBTT increase at 550 °C and beyond (Fig. 5b). Klueh et al. also indicate that thermal aging studies on T91 up to 50000 h result in sharp increase in DBTT at 482, 538 and 593 °C with little change in strength [181].

Several microstructural interpretations can be found in literature. The precipitation of new phases or the coarsening of existing ones, potentially accelerated by irradiation, may act as crack initiator or promote crack propagation [183]. For example, both Mo and W lead to Laves phase formation in a given time-temperature domain (as shown in Fig. 5c in the case of F82H), which has been identified as the main reason for embrittlement in RAFM steels [156,177]. De Carlan et al. report that Laves phase appear as thin films engulfing carbides along grain and lath/subgrain boundaries in a W-rich RAFM steel after 10000 h at 550 °C [184]. The amount of Laves phase formed can be reduced by reducing tungsten and molybdenum concentration. Besides, thermodynamic simulations are a useful tool to predict the amounts of precipitates at equilibrium and to compare them to experimentally extracted amounts, such as in Ref. [156]. They can also be used to determine optimized chemical compositions to minimize the effect of precipitation on properties during elevated-temperature exposure.

Segregation phenomena are also reported in literature. Fernandez et al. observe a chromium enrichment at grain boundaries due either to the presence of Cr-rich carbides, or to chromium segregation, during thermal aging of EUROFER97 between 400 and 600 °C up to 10000 h [178]. Phosphorus segregation is also present at grain boundaries after aging at 500 °C, with no proven influence on the mechanical properties. The DBTT increase after 600 °C/10000 h in Ref. [178] is attributed to recovery or recrystallization, that is, to the lath transformation into sub-grains after long-term aging due to carbide coarsening and unpinning of lath boundaries.

4. Codification

The design and construction of components for nuclear power plants rely on baseline documents such as the American ASME Boiler and Pressure Vessel Code [185], the Japanese JSME Code for Nuclear Power Generation Facilities [186], or the European RCC-MRx code [187]. These codes are based on established national or international standards, on a set of rules translated from the state-of-the-art knowledge and know-how, and on the experimental feedback from the operation of existing nuclear facilities. Their use guarantees that the mandatory quality and safety requirements are achieved, with regards to materials specifications, joining procedures, allowable limits and operation guidelines. They represent the regulatory framework for discussion between the different participants, suppliers, researchers, designers, manufacturers and safety authorities.

All codes need to be improved in order to meet the requirements of future fission and fusion power plants. Some advanced design concepts, in particular for ITER and for other advanced fusion systems, are either not completely defined or they imply fabrication routes and operating conditions that are not yet incorporated in existing codes. TBM modules for example are geometrically complex, involving state-of-the-art joining technologies, together with relevant Non Destructive Examination techniques, that have not been nuclear qualified [188]. The integration of a new material in a nuclear code may also constitute a key challenge. New materials must be licensed to be used in future fission and fusion reactors, which means that an extensive database needs to be built on appropriate products regarding relevant thermal and mechanical properties, for base metal and weldments (example of EUROFER97 in Ref. [189]). The final qualification steps may go through the fabrication of well-conceived mock-ups and their test in operation conditions as close as possible to the in-service thermo-mechanical loadings and environments. In-service surveillance programs are also intended to validating the materials properties and following their ageing process in actual conditions.

Hence the codification of FM steels requires material specifications, qualification of fabrication procedures, mechanical databases, assessment of allowable limits and adjustment of design rules. The major existing codes have implemented at least two FM steels. ASME Grade 91 is codified in the ASME Code Section III Division 5 [136]. T91 is also implemented in the JSME code and in the European RCC-MRx. EUROFER97 has recently been the second FM material to be included in the RCC-MRx code, under the Section III Tome 6 “Probationary Phase Rules”, for the design and manufacturing of TBM concepts and, on a longer term, of the blankets for DEMO, the fusion Demonstration Power Plant [190].

The incorporation of FM steels in nuclear codes requires the generation or the assessment of design rules adapted to the material behavior under expected loading conditions. The damage modes expected in fission and fusion structural materials may be due to various loading conditions, such as fatigue and creep-fatigue due to pulsed operation, long term creep due to power plant life duration extension or rapid loading due to disruption. As pointed out by the fusion community [122,191,192], embrittlement induced by the combined effects of displacement damage by 14 MeV neutrons and the production of high amounts of helium and hydrogen isotopes are of great concern. The use of a future dedicated fusion material neutron source is needed for the final validation and licensing process, with an envisioned international collaboration for the construction and operation of such a facility.

For FM steels nuclear applications, another key point is the incorporation of the cyclic softening of these steels, whereas most design rules have been drawn from cyclic hardening materials behavior. Careful attention must be given to the effect of pre-cycling on tensile and creep properties - thus on allowable stresses -, to ratcheting rules or to the creep fatigue interaction diagram. Both ASME and RCC-MRx codes use similar rules to evaluate the creep-fatigue damage, by evaluating separately fatigue and creep damages. The choice of the interaction diagram was for a while more severe in ASME code than in RCC-MRx [45], but in 2013 a creep-fatigue damage envelope similar to the one in RCC-MRx was implemented in ASME code, allowing more reasonable evaluation and widening the design window [136]. In addition, fusion

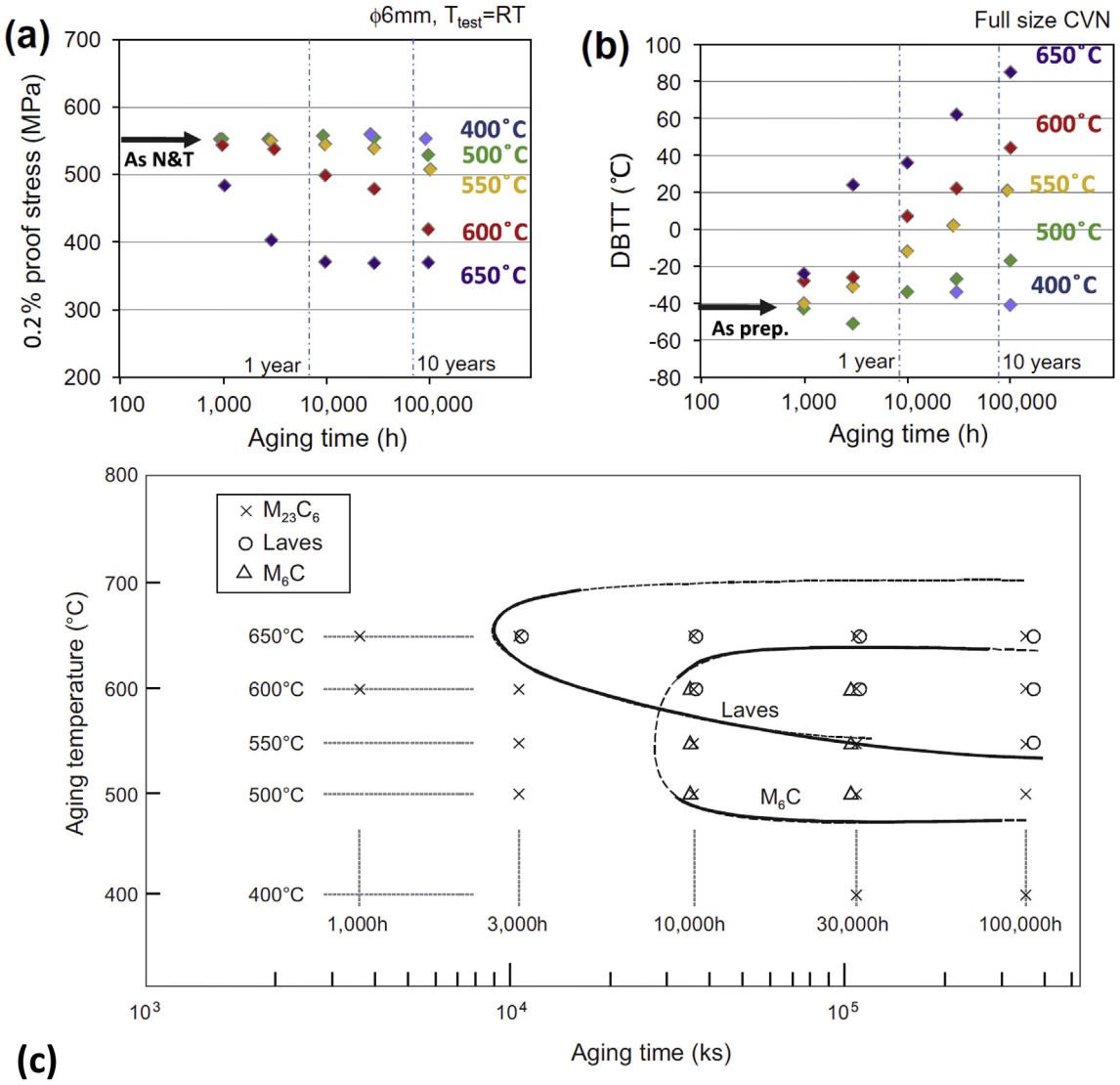

Fig. 5. Aging effects on (a) yield stress and (b) DBTT of F82H steel [182], Time-Temperature-Precipitation (TTP) diagram of F82H steel based on XRD analyses on extracted residue (c) [177].

applications gave the opportunity to re-examine existing rules to accommodate creep-fatigue interactions, and recent improvements in the calculations of creep and fatigue damages have been develop to reduce conservatism in design [193].

Finally, with all the prescriptive R&D and codification work as a background, examples of design studies with FM steels can be found in literature, as in the case of the optimization of SFR secondary hot piping [194]. Ancelet et al. analysis is based on the creep-fatigue diagram and the application of the 2007 edition of RCC-MR code. The aim is to reduce the size of the loops by taking advantage of the better thermal properties of T91 as compared to austenitic stainless steel. Indeed the stress state due to mechanical and thermal loading is proven to be lower in T91 at intermediate temperatures, but at higher temperature in this particular case, the benefit of using T91 is reduced due to its lower creep properties.

5. Irradiation effects in ferritic martensitic steels

The exposure to high neutron loads will inevitably lead to the degradation of the mechanical properties of FM steels as a consequence of the evolution of displacement damage and due to the generation of gaseous transmutation products e.g. helium, see e.g. Refs. [195,196] and references therein. A thorough characterization of the FM steels under application relevant conditions is one of the prerequisites for safe design and operation of future nuclear systems. While irradiations effects in the materials for application in advanced fission energy systems can be studied in a straightforward manner using fission reactor irradiation experiments, see e.g. Refs. [197–200], the adequate characterization of the fusion relevant materials is not yet possible due to absence of an experimental facility with a fusion reactor relevant neutron spectrum, a so-called Fusion Neutron Source (FNS), characterized by high flux of 14 MeV neutrons. As a result, the influence of the neutron irradiation on the performance of fusion structural steels is often studied in fission reactor irradiation experiments, see e.g. Refs. [201–213,123,215,216]. For more recent reviews of the impact of neutron irradiation on the microstructure and mechanical properties of FM steels, the readers are referred to Refs. [195,196,217,218].

5.1. Microstructure evolution

The investigation of neutron irradiation induced microstructural defects in FM steels has been a subject of numerous works, see e.g.

Refs. [25,219–231]. Depending on the irradiation conditions the synergistic effects of displacement damage and transmutation reactions will lead to alteration of precipitate and network dislocation microstructure, formation of dislocation loops, formation of voids and precipitation of new phases as well as to segregation of the alloying and trace elements to the grain boundaries.

The dislocation loops with (a/2)<111> and a<100> type Burgers vectors formed under irradiation are believed to strongly degrade the mechanical properties of FM steels. The inside-outside contrast analysis of the dislocation loops revealed their interstitial nature [221]. Because of the characteristic black contrast observed under bright field Transmission Electron Microscopy (TEM), these defects are often called black dot damage in the literature. For the defect sizes above 1 nm, characteristic dislocation loop contrast varying with the diffraction condition can be resolved by TEM. Whereas the bright field images can be used for the qualitative analysis of the dislocation loops, the weak-beam dark-field images are preferred for the detailed quantitative characterization of the size distribution of the dislocation loops, see e.g. Ref. [226]. In spite of large efforts, there is still no definite conclusion regarding the relative fractions of (a/2)<111> and a<100> loops, see e.g. Ref. [231] and references therein. In fact, by analyzing the visible dislocation loops in fusion steel EUROFER97 after neutron irradiation to 15 dpa at 330 °C in BOR 60 reactor a<100> loops were found to be dominant with a number fraction of 72% [231]. This observation was in accordance with the results on EUROFER97 after irradiation to 15 dpa at 300 °C in HFR reactor, where a comparable a<100> loop fraction of 77% was estimated. With increasing the damage dose to 32 dpa at 330 °C in BOR 60, however, a<100> loop fraction was reported to decrease to 27% [231]. The total density of visible dislocation loops in EUROFER97 after BOR 60 irradiation was increased from 6.9×10^{21} to 8.3×10^{21} $1/m^3$ with increasing the damage dose from 15 to 32 dpa. The average size of the dislocation loops was decreased from 6.1 to 5.1 nm. Dislocation loop microstructure is very sensitive to the irradiation temperature. After irradiation of EUROFER97 in HFR reactor, the loop density was shown to decrease from 4×10^{21} $1/m^3$ to 3×10^{20} $1/m^3$ when the irradiation temperature was increased from 300 °C to 350 °C [225]. The further increase of the irradiation temperature to 450 °C resulted in an even lower density of the dislocation loops of 1×10^{19} $1/m^3$ [225]. This behavior correlates well with the irradiation temperature dependence of the yield strength increase indicating a key contribution of the dislocation loops to the hardening to be discussed in the subsequent section.

In addition to dislocation loops, irradiation may also induce the formation of voids in FM steels. The typical temperature range in which void formation is observed is above 400 °C. The void induced swelling in FM steels in a temperature range between 430 and 470 °C will be discussed later in a dedicated section. The presence of micro-voids has also been reported at the lower temperature range below 400 °C. In EUROFER97 after irradiation in BOR 60 reactor to 15 dpa and 32 dpa at 330 °C [226], the mean void sizes were between 1.6 and 2.6 nm and their densities were at least one order of magnitude lower than the density of the dislocation loops measured for the same irradiation conditions [226]. The neutron irradiation of the same material in HFR reactor to 15 dpa at 300 °C lead to a higher void density of about ~6.5×10^{21} $1/m^3$ [230], which was attributed to the generation of about 10 appm He due to the transmutation of trace element boron.

The stability of precipitates is a key issue for the mechanical properties of FM steels, as they are precipitate-strengthened materials. In addition to ballistic mixing, high energy neutron irradiation induces accelerated diffusion, and this may enhance precipitation, coarsening or lead to the dissolution of precipitates under neutron flux. The stability of $M_{23}C_6$ and MX precipitates has been investigated under various neutron irradiation conditions. Slight coarsening of precipitates in EUROFER97 following irradiation in BOR 60 reactor has been reported in Ref. [230]. A somewhat lower level of coarsening was observed after irradiation in HFR reactor in the same work. Overall, the contribution of the precipitate coarsening to the hardening was estimated to be negligible for EUROFER97. Carbide coarsening was also observed in PNC-FMS irradiated to high doses at temperatures above 400 °C [232]. The size distributions of $M_{23}C_6$ on different boundaries were analyzed in F82H, JLF-1 and 9Cr2WVTa after irradiation in HFIR up to 5dpa at 300 °C. In F82H, $M_{23}C_6$ on large angle boundaries showed a tendency to coarsen, while the general tendency for all precipitates in JLF-1 and 9Cr2WVTa was to shrink [233]. In addition, XRD analyses on extraction residue on these irradiated RAFM steels suggested that MX might have dissolved [234]. Depending on temperature and damage rate, amorphization phenomena were also observed. For instance, amorphization of $M_{23}C_6$ in F82H irradiated in SINQ up to about 10 dpa at temperatures below 235 °C was reported in Ref. [235]. Likewise, Ni doped F82H showed significant amorphization of $M_{23}C_6$ after irradiation in HFIR even at 300 °C [234].

The formation of new phases may also occur in FM steels during irradiation, either due to accelerated diffusion or irradiation-induced mechanisms. For instance the presence of small G-phase particles was reported in HT9 following neutron irradiation in FFTF to 155 dpa at 443 °C [25]. In T91 and NF616 (9Cr-1.8W0.5MoVNb) irradiated to 4.3 dpa at 469 °C, irradiation induced in T91 the precipitation of a new phase, possibly σ phase, while radiation enhanced MX to Z phase transformation was observed in NF616 [236]. The intermetallic χ phase was also found in irradiated FM steels [200,237,238].

α′ precipitation was reported in FM steels under irradiation, including at low temperatures (typically below 450 °C), where it was never observed under thermal aging due too slow precipitation kinetics. For example, α′ precipitates were detected in irradiated 12% Cr HT9 [25,220,238]. The α-α′ phase separation in neutron irradiated 9-12Cr FM steels was also studied in Ref. [222] using Small Angle Neutron Scattering (SANS). In F82H, no α′ phase formation was observed following neutron irradiation to 0.7 dpa and 2.9 dpa at 325 °C, while in T91 irradiated to 0.7 dpa at 325 °C the analysis of the SANS data suggested the presence of α′ precipitates. In Cr-rich materials, HT9 and MANET II (10.5Cr-0.5Mo), the formation of α′ precipitates was found after irradiation to 0.7 dpa at 325 °C. The α′ volume fraction increased with increasing dose and Cr content, and with decreasing irradiation temperature. The authors estimated the Cr threshold concentration in the ferrite for α-α′ unmixing to be 7.2 at.% Cr at 325 °C and 8.3 at.% Cr at 400 °C [222]. It should be noted that no chromium rich α′ precipitates could be resolved in EUROFER97 following HFR or BOR 60 irradiations [226,230,231] by using scanning TEM (STEM) mode in combination with EDX. Furthermore, no sign of α′ precipitates were found in SANS investigations in Ref. [229]. Contrary to TEM and SANS studies, 3–5 nm clusters enriched in chromium, manganese, and silicon atoms were found with a high number density of 10^{24} $1/m^3$ in the same material after BOR 60 irradiation to 32 dpa at 330 °C by using Atom Probe Tomography (APT) techniques [227], indicating that STEM with High Angle Annular Dark field (HAADF) detector might not be sufficient for the resolution of potential nuclei for α' precipitates.

The thorough investigation of Radiation-Induced Segregation (RIS) is crucial as this phenomenon may lead to the degradation of the corrosion performance of the material due to changes of the local chemistry in the steel. Investigations of Prior Austenite Grain Boundaries (PAGBs) in EUROFER97 after irradiation to 32 dpa at 330 °C revealed the increase of the Cr concentration at PAGB by up to 3.4 wt% in comparison to the surrounding matrix [239].

Systematic analysis of RIS in four FM alloys: T91, HCM12A (11Cr-2WMo), HT9, and a Fe-9Cr model alloy following 20 MeV proton irradiations over a range of doses (1–10 dpa) and temperatures (300–700 °C) was done in Ref. [240]. Chromium was found to enrich at PAGBs in all conditions with the exception being T91 irradiated to 3 dpa at 700 °C. The magnitude of enrichment was small (<2 at%). Cr enrichment at packet boundaries in T91 and NF616 irradiated in ATR at 469 °C was also reported in Ref. [236]. RIS of Cr in FM steels was modelled by Wharry and Was using the inverse Kirkendall mechanism [241]. Their model was found to be in good agreement with the experimental observations, i.e. Cr depletion at sinks due to negative coupling with vacancies, the dominant mechanism at high temperature, and enrichment due to positive coupling with interstitials below a threshold temperature. The model also correctly reproduced the experimentally observed lower magnitude of Cr enrichment with increasing bulk Cr concentration.

The quantitative assessment of the influence of the neutron irradiation induced alteration of the microstructure on the mechanical properties is not straightforward due to very complex nature of the radiation damage in FM steels. More experimental and modelling activities are required in order to fully understand the evolution of the microstructure and its impact on the overall performance of the structural steels.

5.2. Irradiation embrittlement

The ductile to brittle transition temperature (DBTT) of the FM steels and the upper shelf toughness can be severely degraded under neutron irradiation. The shift in the DBTT is very sensitive to the neutron irradiation temperature. Strong embrittlement of 8–10%Cr FM steels below 340 °C is often referred to as the low-temperature embrittlement in the literature. Fig. 6a summarizes the shift in the DBTT as a function of irradiation temperature for selected FM steels after neutron irradiation in different Material Test Reactors (MTRs) [123,202,205,208,210,211,215,242–273]. Large shifts in the DBTT are observed after irradiation at temperatures between 250 and 400 °C. In contrast, at irradiation temperatures above 400 °C the shifts in the DBTT are considerably reduced. The observed behavior is attributed to a substantial recovery of displacement damage at elevated temperatures. For RAFM steel e.g. EUROFER97 the DBTT shifts are at most of the order of 50 °C after neutron irradiation to 15 dpa at and above 350 °C [208]. Due to this moderate embrittlement, the temperature window of operation between 350 and 550 °C is recommended for RAFM steels [195,196]. The study of low temperature embrittlement with irradiation dose was a subject of several investigations [205,207,208,211,215]. Fig. 6b summarizes the measured DBTT shifts as a function of irradiation dose (log scale) after neutron irradiation at around 300 °C. Commercial alloys and early stage RAFM steels show larger DBTT shifts than EUROFER97 and F82H already at damage doses below 3 dpa. The shift in DBTT for EUROFER97 and F82H was shown to increase steeply with the dose at damage doses below 15 dpa. At elevated damage doses, the rate of the embrittlement per dose increment is considerably reduced and the DBTT tends towards saturation at the highest achieved damage doses of 70 dpa [195,196]. T91 steel shows the largest embrittlement with a DBTT shift of almost 310 °C after irradiation to 70 dpa at 325 °C (Fig. 6b) [215]. Remarkably, such large embrittlement was accompanied by a drop of the upper shelf energy (USE) quantified by Charpy impact tests on KLST specimens from 7.5 down to 1 J [215]. Comparatively, the USE of 70 dpa irradiated EUROFER97 remained above 6 J [123]. The superior impact properties of EUROFER97 steel after irradiation to 15 dpa at 300 °C over another commercial FM steel MANET I (11Cr-NiMoVNb) was also reported in Ref. [208].

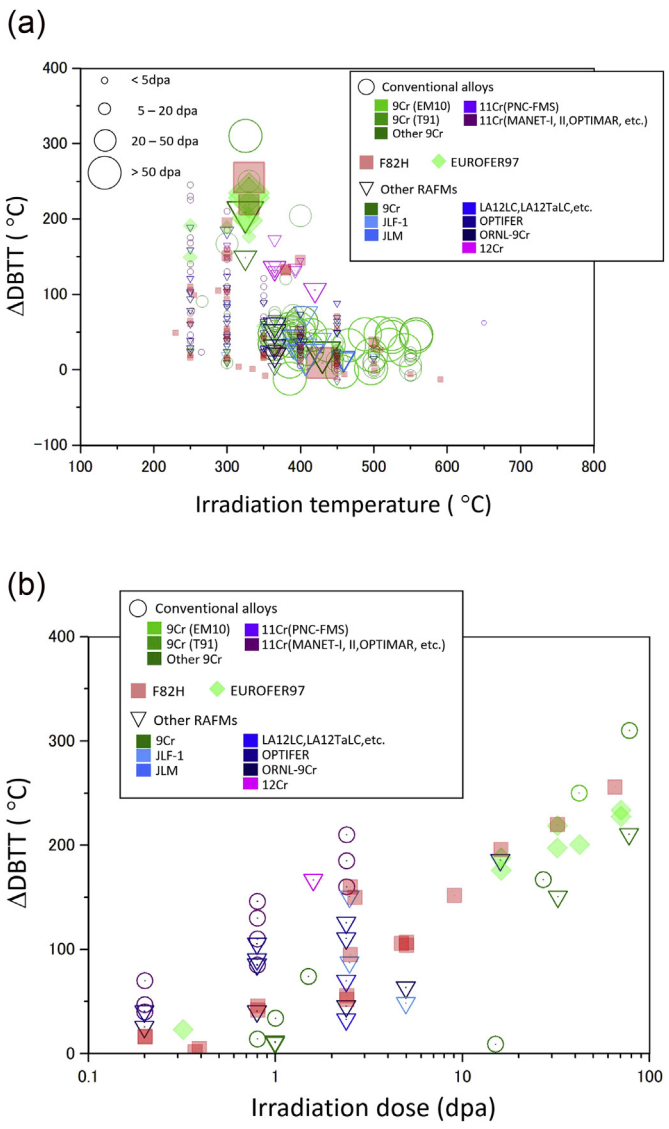

Fig. 6. The shift in the ductile to brittle transition temperature of FM steels as a function of irradiation temperature (a), and as a function of irradiation dose at 300 °C (b) after neutron irradiation in different MTRs [123,202,205,208,210,211,215,242–274]. The DBTT is quantified on miniaturized Charpy impact specimens of KLST type.

5.3. Irradiation hardening

As in the case of the impact properties, the tensile properties of FM steels may be severely degraded under neutron irradiation. Fig. 7 shows the neutron irradiation induced hardening of selected FM steels quantified as an increase in 0.2% proof stress after neutron irradiation in different MTRs [123,210,212,215,254,263,266,268,271,275,277,279–281,283]. The irradiation temperature plays an important role in the evolution of the yield stress. Neutron irradiation at temperatures below 350 °C leads to a strong increase in the yield stress referred to as low-temperature hardening. With increasing damage dose, the neutron irradiation induced hardening increases steeply below 10–15 dpa and tends towards saturation at the achieved damage doses of 70–80 dpa [195,196], indicating that the irradiation-induced microstructure has reached a steady state. The hardening measured on commercial FM steels is, however, considerably larger than the hardening of RAFM steels after

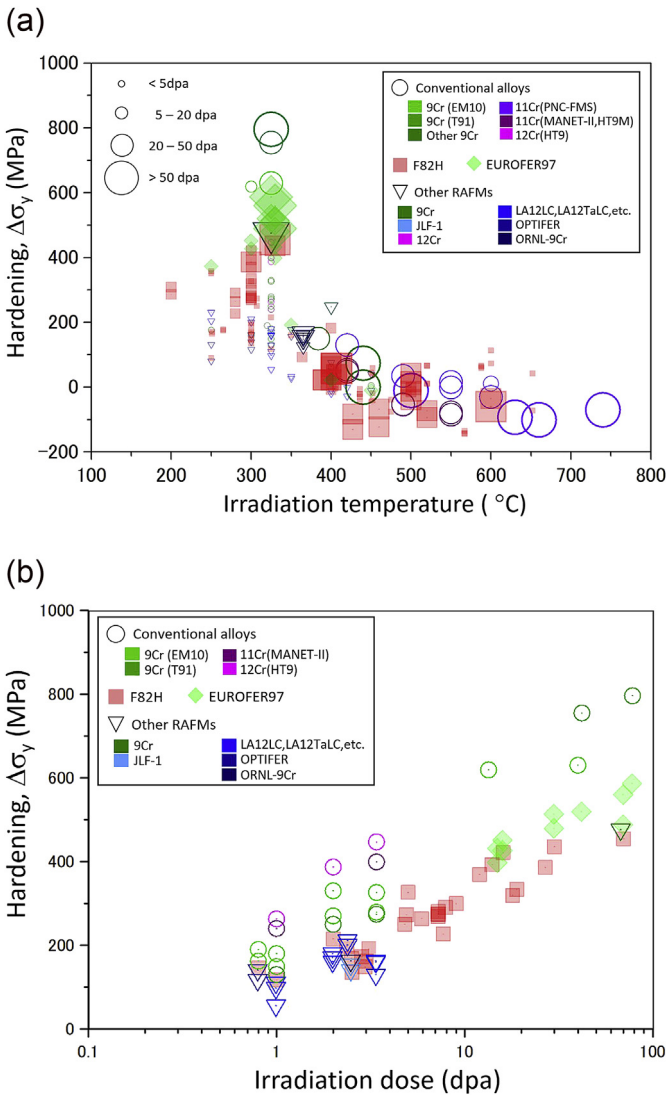

Fig. 7. Neutron irradiation induced hardening of FM steels as a function of irradiation temperature (a), and as a function of irradiation dose at ~300 °C (b) after neutron irradiation in different MTRs [123,210,212,215,254,263,266,268,271,275,277,279–281,283].

irradiation at comparable doses. The largest hardening (up to 800 MPa) is observed for T91 following irradiation to 78 dpa at 325 °C. Neutron irradiation at temperatures of 400 °C and above (Fig. 7a) leads to only minor hardening of the material. Such a strong suppression of hardening correlates with the suppression of embrittlement in Fig. 6a and indicates substantial recovery of the displacement damage at elevated temperatures. Moreover for selected materials, see also [196], a softening is observed at $T_{irr} = 400$ °C which can be attributed to an onset of accelerated aging under neutron irradiation. It has to be noted that no degradation of the tensile properties of EUROFER97 was detected after thermal aging up to 10000 h between 400 and 600 °C [178]. The estimation of hardening shift coefficient C defined as $C = \Delta DBTT/\Delta\sigma$ at irradiation temperatures $T_{irr} \leq 350$ °C for a number of reduced activation FM steels yielded $0.17 \leq C \leq 0.53$ °C/MPa in Ref. [208] which was found to be in a good agreement with the analysis of larger database on 7–9% Cr RAFM steels yielding $C = (0.38 \pm 0.18)$ °C/MPa [282] and indicated that the embrittlement is dominated by a hardening mechanism. The hardening shift coefficient increased at $T_{irr} = 400$ °C which suggested a non-hardening embrittlement (NHE) mechanism that primarily occurs due to aging conditions [208].

5.4. Elongation properties

The low temperature hardening shown in Fig. 7 is accompanied by a strong degradation of the ductility properties [195,212,213,215,254,263,264,266,268,271,275,284–287]. The uniform elongation of FM steels falls below 0.5% already after few dpa. This behavior linked with a strong suppression of the strain hardening capability is believed to be correlated with the localization of inelastic deformation in irradiated FM steels [284]. For the case of EUROFER97, it was furthermore shown that a roughly linear relationship of the type $A_g=(1-R_{p0.2}/R_m)$ holds between the uniform elongation A_g and the strain hardening capability $R_{p0.2}/R_m$ [195]. As for the total elongation, this property remains at an acceptable level of above 5% for RAFM steels even after neutron irradiation up to 80 dpa, see Fig. 8. The commercial FM steels, e.g. T91, show somewhat lower total elongation already in the unirradiated state, and it drops below 3% after irradiation to 78 dpa at 325 °C [215]. At irradiation temperatures above 350 °C, the degradation of the total elongation decreases with increasing T_{irr} and disappears almost completely at $T_{irr} = 450$ °C [275]. This behavior indicates substantial annealing of the neutron irradiation induced displacement damage at elevated temperatures and correlates with reduced hardening and embrittlement.

5.5. Swelling

One of the prerequisites for the application of FM steels in advanced fission and fusion nuclear systems is a good swelling resistance due to the high damage doses to be received by the materials. The swelling resistance of FM steels is superior to the swelling resistance of austenitic steels under fast reactor irradiations, see Ref. [288] and references therein. The austenitic steels were reported to exhibit a universal steady-state swelling rate of ~1%/dpa at irradiation temperatures above 430 °C [288]. On the other hand, very long transient regimes were reported, and swelling rates of ~0.2%/dpa or greater were anticipated for FM steels in the same work [288]. Extensive investigations of fast neutron irradiation induced swelling in FM steels have been done

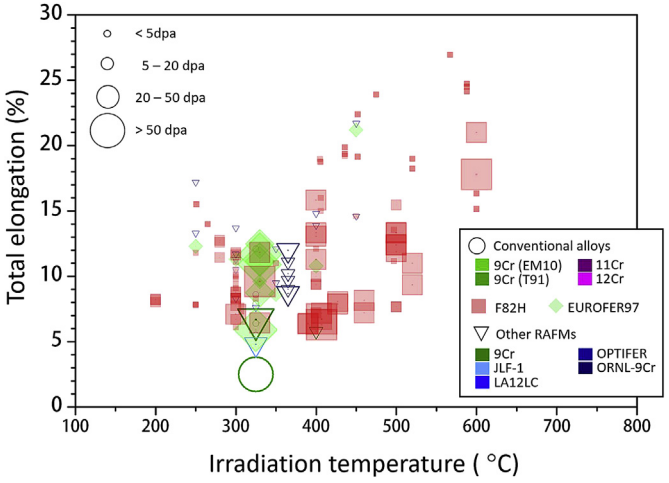

Fig. 8. Total elongation of FM steels as a function of irradiation temperature after neutron irradiation in different MTRs [195,212,213,215,254,263,264,266,268,271,275,284–287].

in the past either by measuring the dimensional or density changes of the samples [199,219,289,290], or by the determination of void swelling via TEM studies [198,200,228,237,238,291–295]. Selected results from these investigations are summarized in Fig. 9. Even at the highest achieved doses of 208 dpa the volumetric swelling is below 3% for T91 and even lower for HT9. The swelling rates ≤0.012%/dpa were estimated in HT9 and 9Cr-1Mo steels irradiated to 208 dpa at 400 °C [290]. RAFM steels such as F82H and JLF irradiated up to 70 dpa show volumetric swelling below 0.15 and 1%, respectively, which are comparable to the swelling values measured on commercial FM steels, e.g. EM10 or EM12. The superior swelling resistance of FM steels is often related to the lower dislocation bias (preferential absorption of interstitials in comparison with vacancies) and the higher self-diffusion in FM steels compared to austenitic steels [296]. In Ref. [297] it was argued that the metallurgical microstructure was responsible for the good swelling behavior of FM steels rather than the crystallographic structure. Prior austenite grain boundaries together with sub-grain and lath boundaries, $M_{23}C_6$ and MX precipitates and high dislocation densities are believed to act as defect annihilation sites and thus contribute to the swelling resistance of FM steels. In fact FM steels subjected to a tempering treatment at a low temperature (700 °C), containing relatively high densities of small precipitates and a high density of line dislocations were found to show lower swelling rates than the FM steel subjected to higher temperature (760 °C) tempering heat treatments [297]. Furthermore, in 12%Cr FM steels with a duplex microstructure subjected to high dose ion irradiations, TEM investigations have revealed higher swelling levels in ferrite grains compared to tempered martensite grains, which is a further indication of the beneficial effect of the martensite microstructure on the swelling resistance [69,298].

Generation of the transmutation gas helium under fusion relevant conditions may substantially modify both the incubation time and the steady-state swelling rates of FM steels. The comparative studies of void swelling in F82H steels doped with different contents of natural boron and separated 10 boron isotopes in Ref. [295] indicated enhancement of void swelling due to helium. After irradiation to 51 dpa at 400° of natural boron (0.0060%) and ^{10}B isotope (0.0058%) doped F82H, the average void swelling values of 1.2% and 1.1% were determined, with corresponding helium contents of 80 and 330 appm He, respectively. The swelling was about two times larger than the void swelling of 0.52% measured in standard F82H steel where about 25 appm helium was generated due to transmutation of the trace element boron. This experiment does indicate a reduction of the incubation time for the void nucleation due to transmutation gas helium. However, a very high helium production rate characteristic of the boron doping technique at an early irradiation stage below 1 dpa, e.g. about 305 appm He/dpa in the case of F82H steel doped with 0.0058% 10B isotope, does not allow direct transferability of these results to fusion conditions.

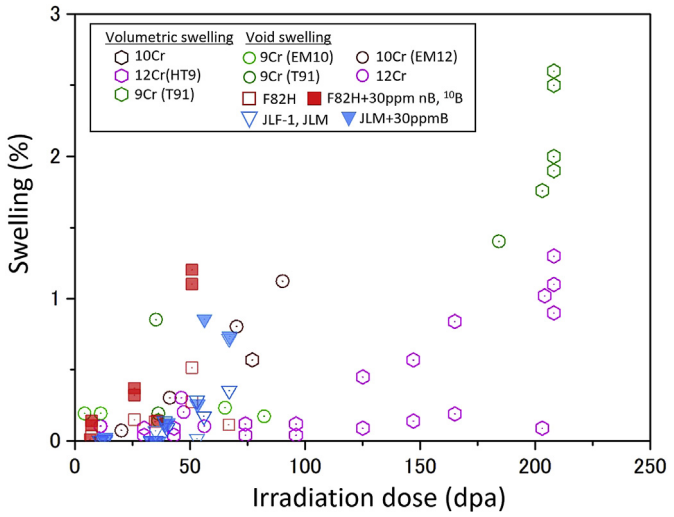

Fig. 9. Swelling of FM steels as a function of the damage dose for neutron irradiation temperatures between 365 and 600 °C. The results stem from Refs. [198–200,219,228,237,238,289–295]. The swelling was directly determined either by measuring density or volumetric changes of the samples or estimated by determining the void volume fraction using TEM.

The void swelling behavior and particularly the influence of transmutation gases helium and hydrogen on the microstructure is often simulated by surrogate ion irradiation experiments, see e.g. Refs. [298–305]. By tuning the fluxes, fluences and energies of the implanted ions, gas atom to dpa ratios characteristic of fission or fusion operational conditions can be emulated. Furthermore, damage accumulation rates up to four orders of magnitude larger than material testing fission reactors can be achieved at considerably lower costs.

Fig. 10 shows volumetric swelling determined in selected FM steels following either simultaneous dual beam irradiation or after single ion irradiation of helium pre-implanted samples [298–301,304,305]. In the case of F82H, a swelling peak of about 0.6% was reported at 430 °C after simultaneous irradiation with iron and helium to 50 dpa at fusion relevant helium to dpa ratios [301]. Other fusion type steels JLF-1 and JLS-1 exhibited swelling peaks at a somewhat higher temperature of 470 °C for comparable helium to dpa ratios [299,300]. Higher swelling values compared with F82H may be attributed to higher damage doses between 60 and 125 dpa reached in the case of JLS-1 steel.

The high damage accumulation rates characteristic of ion implantation experiments have to be properly taken into account to predict the material behavior under fission or fusion neutron spectra. A comparable void swelling was reported in Ref. [302] in HT9 after neutron irradiation in the Fast Flux Test Facility (FFTF) to 155 dpa at 443 °C and after Fe^{2+} ion irradiation to 188 dpa at 460 °C. In the latter case 1 appm He was pre-implanted to simulate the transmutation gas effects. Furthermore, in the same work, the size and density of precipitates and loops following ion irradiation within a factor of two of those for reactor irradiation were reported. A temperature shift of about 70 °C was identified in Ref. [303] by comparing the microstructure of EUROFER97 after irradiation to 26 dpa at 400 °C with 3 MeV Fe^{+} ions with the microstructure of EUROFER97 after neutron irradiation to 32 dpa at 330 °C [226]. In Ref. [305] by comparing the helium bubble microstructure, density of dislocation loops and hardening of dual beam irradiated EUROFER97 with those of neutron irradiated boron doped model alloys [223,225,306] dose rate effects were identified and associated with a temperature shift of 50°–70 °C. Extensive comparative studies and accompanying modelling will be required in the future to predict the dose rate effects in FM steels.

5.6. Irradiation creep

Irradiation-induced creep will play an important role in the relaxation of the thermal stresses occuring in nuclear reactor components. Due to this reason, the assessment of irradiation creep effects is mandatory for the safe design of advanced nuclear energy systems. Irradiation creep is often investigated by irradiating pressurized tubes and the diametral strain is measured at discrete values of accumulated damage dose, see e.g. Refs. [210,307]. Fig. 11 shows the diametral strain rate as a function of hoop stress in a temperature range between 300 and 500 °C. At temperatures below 400 °C thermal creep effects are negligible and the diametral

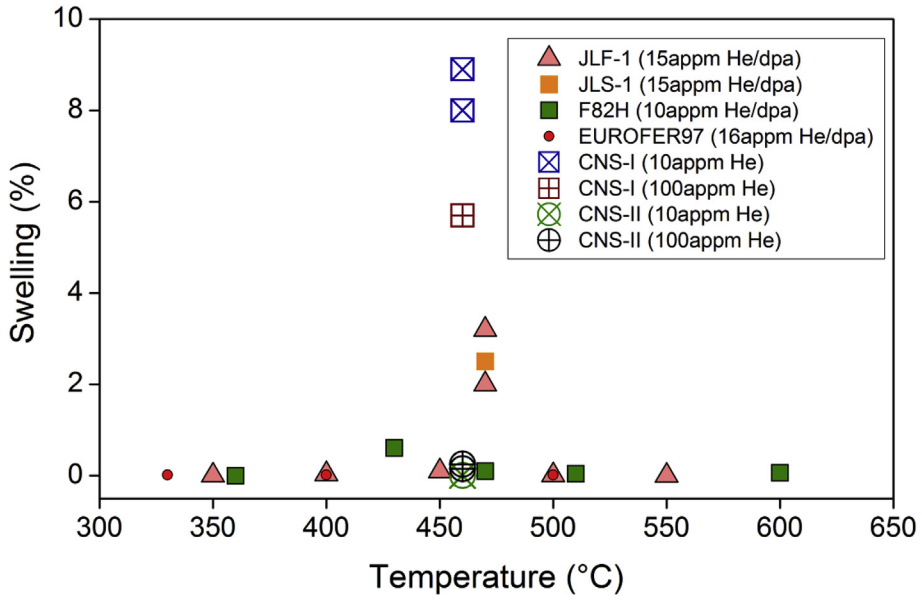

Fig. 10. Void swelling as a function of irradiation temperature in selected FM steels determined either after simultaneous dual beam irradiation experiments or after single ion irradiation of helium pre-implanted samples [298–301,304,305]. Small symbols: < 20 dpa; Medium symbols: 20 < dpa<150 dpa; Large symbols: >150 dpa.

strain rates shown in Fig. 11 can be directly related to the irradiation creep. All investigated FM steels show comparable creep rates at irradiation temperatures below 400 °C. Nearly the same values of the irradiation creep-modulus $A=(0.7\pm0.1)\cdot10^{-6}$ (dpa MPa)$^{-1}$ were reported for EM10, 9Cr2WTaV and EUROFER97 FM steels in Ref. [210]. Irradiation creep of F82H is comparable to that of other FM steels at temperatures below 400 °C. The enhancement of the creep rates of F82H at temperatures above 400 °C is significant at stress levels over 1/3 of yield stress, as shown in Fig. 11. Another indirect method to investigate the irradiation creep behavior is the study of irradiation-induced stress relaxation where bolt or ribbon type specimens are pre-stressed to different levels of stresses, typically between 30% and 90% of the yield stress [308]. The difference in the bolt length and the strip curvature radius is used as a direct measure of stress relaxation under irradiation. The irradiation-induced stress relaxation appeared to be independent on the pre-stress level leading to 42–47% stress retention in EUROFER97 after irradiation to 2.7 dpa at 300 °C [308].

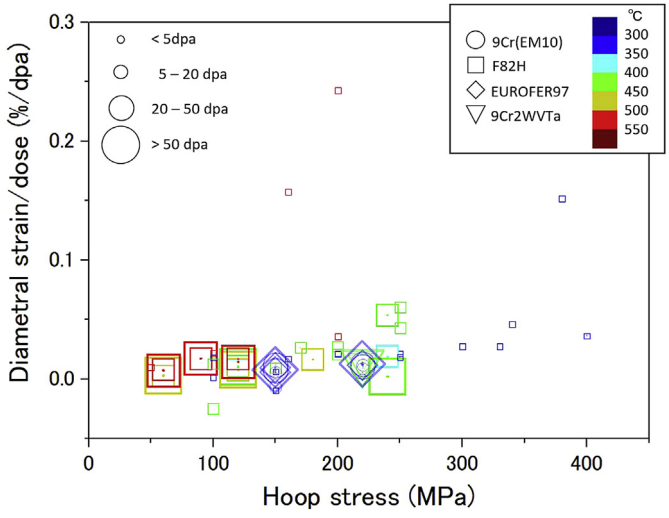

Fig. 11. Irradiation creep rate as a function of Hoop stress between 300 and 520 °C, see color legend for temperature. The results stem from Refs. [196,210,309–311]. (For interpretation of the references to color in this figure legend, the reader is referred to the Web version of this article.)

5.7. Helium effects

The high energy, high-intensity neutron fluxes in the fusion reactor will lead to the production of the gaseous transmutation products helium and hydrogen at levels far beyond the levels generated in MTRs. A detailed calculation of helium production rates at different positions of in-vessel components of a future fusion power plant has been performed in Ref. [312] predicting helium production rates of the order of about 10 appm He/dpa. Various experiments devoted to the study of helium effects on the microstructure and mechanical properties of fusion RAFM steels have been performed in the past using either fission neutron irradiations of nickel or boron doped or ^{54}Fe isotope substituted model alloys [213,223,313–316], or irradiations in spallation target environment [317,318]. For an overview of the limitations of boron doping and spallation target irradiation experiments for the simulation of helium effects, the reader is referred to Refs. [195,196,313].

A significantly larger DBTT shift measured in F82H steel after homogeneous helium implantation at 250 °C in comparison with the DBTT shift observed in F82H after neutron irradiation to the same low damage dose of 0.2 dpa at 250 °C was ascribed to a fracture stress reduction due to helium segregation at fracture surfaces in Ref. [319]. Large extra embrittlement identified in neutron irradiated boron doped model steels in comparison with baseline EUROFER97 was attributed to helium in Refs. [195,314,315]. The DBTT measured in the impact tests was found to increase progressively with increasing helium amount up to 420 appm He at irradiation temperatures below 350 °C [195]. A substantial reduction of helium effects at elevated irradiation temperatures was attributed to rather different evolution of the helium microstructure at different irradiation temperatures in a model steel [314]. Indeed the low-temperature neutron irradiation was shown in Ref. [223] to lead to a homogeneous nucleation of helium bubbles in the steel matrix with some minor fraction

nucleated at the grain boundaries. On the other hand, bubble nucleation was found to be predominantly heterogeneous with the majority of the bubbles nucleated at line dislocations after irradiation at 450 °C, see Ref. [223]. At $T_{irr} \leq 350$ °C and up to 420 appm He, an helium embrittlement rate between 0.5 and 0.6 °C/appm He was estimated from the boron doping experiment [195] which is slightly higher than the embrittlement rate of 0.4 °C/appm He obtained in Ref. [316] at $T_{irr} = 250$ °C up to 300 appm He by applying the boron doping technique to F82H steel. At $T_{irr} = 450$ °C, helium embrittlement rate of about 0.25 °C/appm He was estimated up to 420 appm He in Ref. [195]. It should be mentioned that only a minor influence of up to 420 appm helium on the tensile properties was reported in Ref. [213] at irradiation temperatures between 250 and 450 °C.

The influence of helium on the microstructure and swelling in boron doped 9% Cr RAFM model steels has been thoroughly studied in Ref. [320] after neutron irradiation up to 16.3 dpa. Whereas up to helium contents of 410 appm He no swelling was observed at the irradiation temperature of 250 °C, swelling values between 0.54% and 0.68% were estimated at the irradiation temperature of 350 °C. These values are 3–4 times larger than the swelling of 0.12% observed in EUROFER97 irradiated under the similar conditions indicating promoting of swelling by helium. The spatial distribution of helium bubbles has changed from a random distribution at 350 °C to a heterogeneous distribution at dislocations and grain boundaries at 450 °C. The swelling was remarkably reduced down to 0.09%–0.15% at 450 °C. Comparatively, the production of 5800 appm helium in another experimental boron doped model steel irradiated to the same damage dose induced 0.18% and 0.42% swelling at 300 and 400 °C, respectively. Preferential nucleation of helium bubbles on structural defects was not detected in the latter case [320]. The SANS cross section was found to be substantially increased for neutron irradiated boron doped model alloy with 5600 appm helium in comparison with lower helium content (410 appm) boron doped alloys in Ref. [321]. In addition the magnetic SANS component was strongly reduced. Such effects were attributed to the higher helium densities measured in high boron content steels and to the presence of micro cavities produced after dissolution of large boron carbides. Comparable SANS cross sections for boron doped model steels with produced helium contents of 80 and 410 appm after irradiation at 450 °C in Ref. [321], furthermore, indicated the effect of the helium content below 410 appm to be significantly smaller compared to the dpa one in close agreement with the observation found in Ref. [320].

Some limitations of the boron doping technique such as metallurgical effects of boron, varying helium production rates, uncertain chemical effect of byproduct lithium were addressed in Refs. [195,196,313]. Due to the above limitations, an overestimation of the helium effects is expected in these simulation experiments. Also, the irradiation with spallation protons and neutrons has some limitations. Particularly, very high helium to dpa ratio of about 70appm/dpa and variations of the irradiation temperature due to the periodic variations of intensity of the proton beam have to be emphasized.

Alternative techniques, such as the He injection technique during neutron irradiation utilizing Ni(n,α) reactions by plating NiAl on specimen surfaces may solve some of the above issues [322]. The key issues with this technique are associated with the limited injected zone of He which is just a few μm from the specimen surface.

Though the above mentioned simulation techniques do help to better understand helium effects and provide valuable input for the modelling activities, the availability of a FNS with fusion reactor relevant neutron spectra is mandatory for the detailed investigation of synergetic effects of displacement damage and transmutation gases at fusion relevant dpa and gas production rates and for the generation of the mechanical properties database for DEMO design criteria development.

6. Environmental effects

Design studies for Generation IV projects and fusion systems have triggered R&D programs throughout the world on the chemical compatibility of FM steels with reactor specific environments. In general in steam and in highly oxidizing media, increasing the chromium content makes alloys more corrosion resistant and oxidation resistance of steels goes up dramatically when the chromium content exceeds 20%. Steels will degrade to various degrees and in various ways under the environmental conditions anticipated for advanced reactors: liquid metals such as sodium in SFR, lead and lead alloys in LFR and ADS systems, lithium and Pb-17Li for fusion blanket modules, steam in SFR or LFR steam generators, Super Critical Water in SCWR, gasses such as helium in Gas-Cooled Reactor Systems and Super Critical CO_2 in advanced power conversion systems. In these environments, the maximum temperatures are higher when compared to conventional light water reactors, and the fluids are mostly more aggressive towards materials. Additionally, the fluids in nuclear systems serving for heat exchanges typically operate non isothermally. This imposes a set of additional driving forces for corrosion and mass transfer that can exacerbate degradation and introduce additional reaction pathways. For future fission systems, the Gen IV criteria call for a sixty-year operation. Key elements must be designed and qualified for extended lifetimes, up to 60 years for non-replaceable components. Material qualification must exclude environmentally induced failures and provide conservative corrosion allowance.

6.1. Environment effects in liquid metals

A detailed overview on corrosion phenomena and mitigation strategies in liquid sodium, in lead and in lead-bismuth eutectic (LBE) can be found in Refs. [61,323–325]. SFR are generally designed with a coolant maximum temperature of 550 °C for a core inlet temperature close to 400 °C, but the cladding temperature may go up to about 650 °C. ADS and LFR operate at somewhat lower temperature with a maximum coolant temperature topping at 480 °C.

The main elements of steels, Fe and Cr, are dissolved in liquid metal coolants and the solubility limits increase with temperature. In Fig. 12, the solubility limits are graphically drawn in the temperature range of interest for advanced systems with solubility equations from Refs. [61,323]. The solubility limit of Cr in Na is well below 1 wppm when extrapolated from the high temperature data. It is higher in Pb and in LBE. Note that Ni has the highest solubility of common metallic elements especially in lead alloys. In the pure dissolution regime, when temperature is distributed in a circulation system, the elements dissolved from the higher region (de-alloying) are deposited at lower temperature regions due to supersaturation, and accordingly the so-called mass transfer –dissolution/precipitation– continues with time. Fig. 12 also gives the solubility limit for oxygen, as this minor element largely affects corrosion in liquid metals. Oxygen is highly soluble in Na with a solubility that ranges from 400 wppm at 400 °C to 5500 wppm at 700 °C, but lower than 1 wppm at 110 °C allowing purification by crystallization at low temperature, and above the limit, solid sodium oxides are formed. For technological issues as well as to limit corrosion, oxygen concentration in liquid Na is preferably maintained below ~3 wppm during normal operating conditions [325]. The solubility limit of oxygen in liquid Pb at 500 °C is only about 5 wppm. The formation of solid Pb oxides has to be strictly avoided to prevent

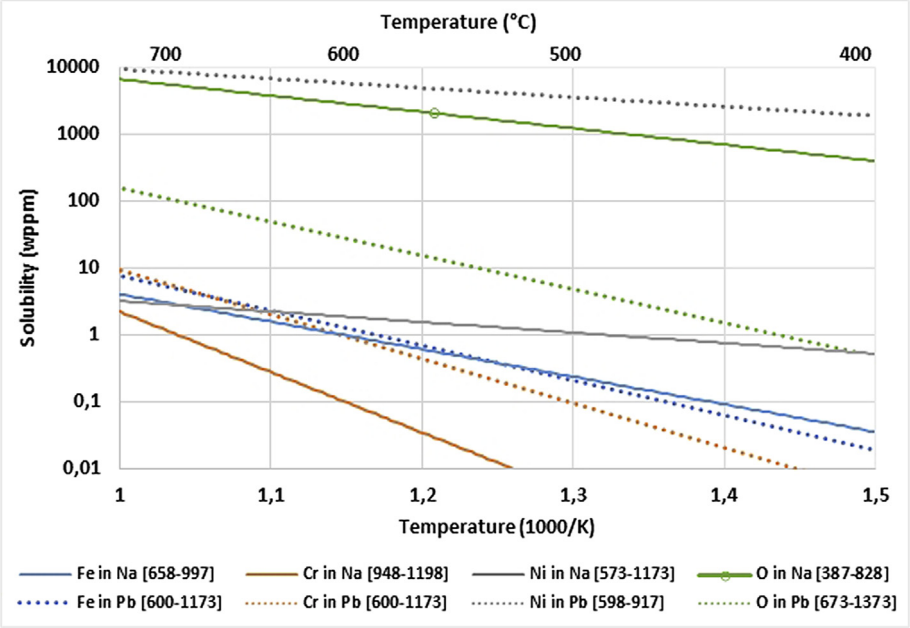

Fig. 12. Semi logarithmic representation of the solubility limits of Fe, Cr, Ni and O in liquid Na (solid lines) [323] and liquid Pb (dashed lines) [61], including the temperature validity domains into brackets.

risks of clogging in the circuits and the lower limit of oxygen is driven by corrosion consideration (see henceforth).

For the corrosion process of alloys, a significant difference between sodium and lead environment is in the stability of oxides formed at the metallic surface. Since the binary oxides (Fe_3O_4, Cr_2O_3…) are readily reduced in sodium by reactive wetting [326], the flowing liquid metal comes into direct contact with the material producing dissolution/reprecipitation of alloy elements from the Na wetted surface.

An example of modified 9Cr steel exposed in static liquid oxygenated sodium at 550 °C is shown in Fig. 13a [327]. Corrosion proceeds by the selective oxidation of chromium at the sodium-steel interface with the formation of:

- nodules or scale of sodium chromite ($NaCrO_2$),
- a chromium depleted zone in the steel where sodium has penetrated.

The Cr-depleted zone exhibits a specific microstructure (martensite tempered laths) and sodium fills the porosity. It is believed that silicon plays a role in that intergranular attack by promoting the formation of mixed Si-Na oxides [323,328]. The mechanism of these oxidation and oxygen-enhanced dissolution is still to be fully elucidated to progress towards predicting the long term steel behaviour under given conditions. The intermediate formation of Na-Cr-O and Na-Fe-O complexes were proposed since the 70's to justify the straight increase of the iron solubility with the oxygen content [329,330]. The apparent solubility of the metallic element Cr or Fe would thus increase due to the formation of composite oxides. Corrosion then tends to be enhanced with an increase of oxygen in Na.

Fig. 13b plots the evolution of the corrosion layer against time for T91 and austenitic stainless steel 316L(N) [17%Cr] [331] in static oxygenated sodium (10–40 wppm) at 550 °C. After 5000 h, the mixed oxide scale is 2.5 times thicker for T91 than for SS 316L(N) and the Cr-depleted layer is 7 times thicker. The FM steel appears to be more prone to selective oxidation in oxygen-containing sodium than the austenitic steel. The corrosion rate of T91 steel would be a few microns per year.

It is commonly agreed that corrosion in sodium with low dissolved oxygen has two stages: the start-up corrosion for several thousands of hours, then the steady-state corrosion that progresses at an approximately constant rate. Thorley and Tysack [332] proposed an equation for evaluating the corrosion rate of structural materials in sodium for a temperature T = 400–650 °C, a fluid velocity of 2–4 m/s and a dissolved oxygen concentration C_O between 5 and 25 wppm:

$$\log V_{corr} = 3.85 + 1.5 log C_O - \frac{3910}{T}$$

with V_{corr}, the corrosion rate in μm/year, and T in kelvin. This equation was successfully applied to FR316 (austenitic) and FM steels for the Monju reactor [324]. This equation shows that the corrosion rate of FM steels in sodium increases with temperature and dissolved oxygen. With the expression above, the conservative material loss by corrosion would be ~4 μm/year for C_O = 10 wppm in flowing sodium at 550 °C. An example is shown in Fig. 13. Even though the empirical equation developed by Thorley appears to satisfactorily reproduced most experimental data, the global mechanism of the metal dissolution in sodium and the specific role of intermediate compound formation (like Na-Cr-O) still needs to be elucidated to develop a sound predictive model on the long term.

Other corrosion phenomena are related to mass transfer and diffusion when sodium flows in a heat-exchanging zone with a temperature gradient or when circuits are made out of different alloys.

Since a FM steel generally contains only a small amount of Ni that is to say a low Ni activity, the dissolved Ni in sodium (for instance dissolved from components in austenitic steel at higher temperature in the same system) may penetrate from the surface and diffuse within the steel, this process being called alloying.

Great emphasis has been placed on carbon transfer as carbon plays a significant role in maintaining steel strength properties [333]. Carbon may be transported by sodium in heat transfer

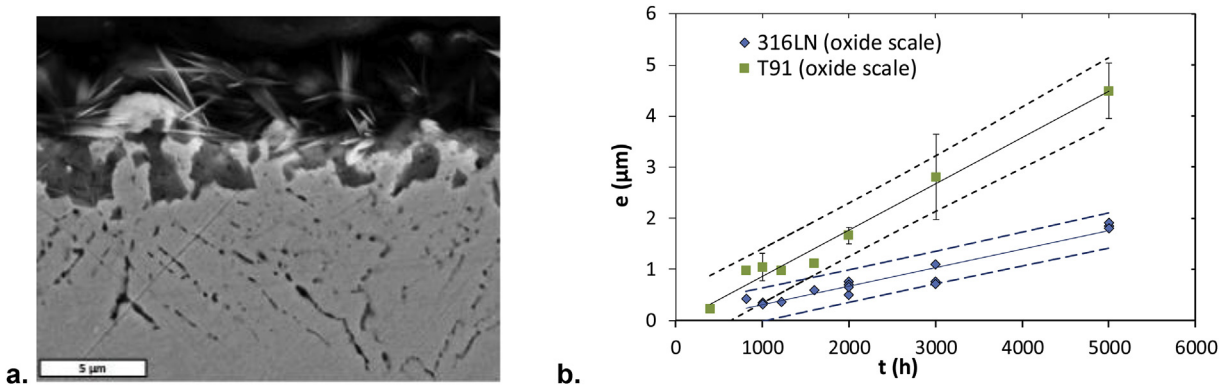

Fig. 13. T91 steel immersed in static liquid sodium with 10 wppm O at 550 °C.
a) specimen surface after 5000 h
and b) evolution of the oxide scale thickness (with 95% confidence hyperboloids) assessed by GD-OES (austenitic SS 316L (N) is shown for comparison) [327,331].

systems because of carbon activity gradients existing between zones at different temperatures or zones made of different steels. The chemical activity of dissolved carbon in sodium relative to the carbon activity in the material determines the direction of the carbon transfer: decarburization or carburization while temperature alters the carbon diffusion rate. Carbon would be transferred from ferritic steels that have a higher carbon chemical activity onto austenitic steels leading to carbon loss and a possible impact on the ferritic steel high temperature mechanical properties. This decarburization has been strongly limited in SFRs by the use of high chromium ferritic steels with relatively lower carbon activity and was proved negligible at 550 °C [334]. Decarburization was only shown to be a serious issue at the highest temperature: for example at 650 °C, creep rupture strength in sodium is reduced compared with that in air [324].

Liquid metal embrittlement (see below) of FM steels with a standard metallurgical state is generally considered negligible in pure liquid sodium (with a low impurity content). Constant-load test conditions, does not produce a measurable effect on the rupture strength even if some (low) susceptibility has sometime been reported at low temperatures [335,336].

Finally, cases of post-operation cracking of FM steels exposed to liquid sodium have been reported in specific conditions and pipe locations, like bends or T-junctions, due to the formation of sodium hydroxide during a shutdown with dripage.

Unlike sodium, lead and bismuth are oxidized for oxygen partial pressures above those for the formation of metallic oxides of Fe and Cr. Following thermodynamics, a metallic oxide layer can be formed at the steel surface in contact with liquid lead and LBE. Therefore in lead and LBE, depending on the dissolved oxygen concentration, two processes are encountered [337]:

dissolution of steel occurs when the dissolved oxygen concentration is below than that needed for iron oxide formation,
oxidation of steel occurs when the oxygen concentration is higher (but lower than the oxygen solubility limit in lead to prevent precipitation of Pb oxides).

The ***dissolution*** mode for 9-12Cr steels is characterized by homogeneous dissolution in the liquid lead metal with no formation of a superficial layer or preferential dissolution of a particular element as shown in Fig. 14a. The solubility limit of Fe and Cr being significantly higher than in alkali metals like sodium or lithium (see Fig. 12) [323], the observed corrosion of structural steels in lead and LBE is severe, although corrosion rate in lead is of slightly lower magnitude. The steel rapidly dissolves in heavy metal liquid with a strong impact of the flow velocity. A large variation exists between experimental data possibly due to inappropriate physicochemical control of the liquid metal and to discrepancies in assessing the weight loss that makes difficult to develop a global empirical correlation. Nevertheless, an average corrosion rate around 100 µm/year can be estimated for 9Cr steels in lead alloys for temperature up to 400–450 °C and a moderate hydrodynamic regime (fluid velocity lower than 2–3 m/s). For temperature around 550 °C, the dissolution rate is of a few hundredth µm/year up to a few mm/year which excludes the use of such steels in these conditions [337].

Consequently, oxygen potential in the liquid lead alloy needs to be carefully controlled and maintained above the concentration needed for magnetite formation at the steel surface.

In addition to pure corrosion, liquid metal embrittlement can occur in low-oxygen liquid metal at lower temperature (<450 °C in LBE). For a ductile material, like FM steels, LME is characterized by a loss in the elongation to failure when stressed while in contact with the liquid metal. This ductility drop can be drastic in liquid lead or LBE. Main factors affecting LME include:

- wetting of the steel surface is a strong prerequisite to LME [326],
- temperature as generally LME is more important around the melting point and decreases when temperature increases,
- the steel microstructure and metallurgical state,
- a load higher that the yield stress,
- impurity contents in the liquid metal: A low oxygen content is required as it allows wetting of the steel surface and prevents the formation of a surface oxide layer,
- irradiation generally enhanced LME; Long et al. [339] observed early failure of irradiated F82H and T91 when tensile tested at a slow strain rate in LBE in the temperature range between 200 °C and 400 °C.

As an example [340], T91 exhibited LME when exposed to liquid lead and LBE in the temperature range 300–450 °C. The heat treatment applied to the steel was shown to strongly influence the sensitivity to brittle fracture. A ductility recovery was observed at temperature higher than 450 °C. Beside a reduction in the tensile total elongation, tests of T91 in LBE showed an alteration of creep and creep to rupture properties, of low cycle fatigue life and of fatigue-relaxation life [61].

For oxygen concentration higher than the one necessary for magnetite formation, 9-12Cr steels will undergo ***oxidation*** with the formation and growth of a thick oxide layer as shown in Fig. 14b. This oxide has a double-layer structure with an outer part made of porous magnetite and an inner Fe-Cr spinel layer [338]. Both layers

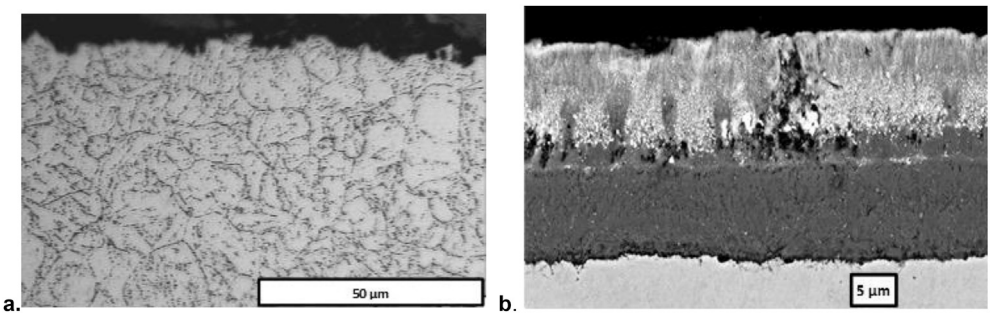

Fig. 14. Cross-section examination of T91 immersed in liquid LBE at 470 °C – a) after 1200 h with 10^{-11}-10^{-12} wt% O and V(LBE) = 0.075 m/s and b) after 3700 h in saturated-oxygen alloy [338].

have a similar thickness and the interface between them corresponds to the original surface between the steel and the liquid Pb(Bi). The nature of these layers remains identical whatever the test temperature between 470 °C and 600 °C [341] but evidence of diffusion of Pb into the external magnetite layer to form a mixed Pb-Fe oxide was gained at 560 °C [342]. In addition, internal oxidation occurred at grain boundaries of T91 at temperatures above 550 °C.

Oxidation rates for FM steels are higher than for austenitic steels. The addition of silicon in a Cr steel (for instance the grade EP823 with 1.3% Si developed in Russia) is beneficial and diminishes the oxidation rate. However, Si addition negatively affects the mechanical properties especially after irradiation.

The oxidation kinetics is parabolic and the oxide layer thickness, h, follows:

$$h = \sqrt{k_p t}$$

with t, oxidation time and k_p, parabolic rate constant. The k_p constant increases with temperature as for a thermally activated process. Flow velocity does not seem to increase the oxidation rate although the outer magnetite oxide layer is eroded at a high flow velocity. Models have been published to predict the oxidation of T91 that capture this parabolic growth. For instance, Martinelli and Balbaud-Célérier have developed a local approach based on the Available Space Model [341]. Fig. 15 shows experimental data and simulations for T91 steel at different temperatures. As seen in Fig. 15, oxidation rate at temperature of 500 °C and higher is significant and the resulting thick oxide layers can interfere with heat transfer. Mitigation strategies are necessary. The most promising ones for FM steels imply surface alloying and coatings [343].

6.2. Environmental effects in steam and supercritical water

T91 steel is the reference choice for straight tube steam generators in SFR or LFR with a typical maximum water temperature of 490 °C and liquid metal up to about 520 °C. This application benefits from the large knowledge of the oxidation behavior of 9-12Cr steels in steam boilers (see e.g. Ref. [344]). The growth of oxide scales on engineering alloys exposed to steam at high temperatures and pressures is an expected and unavoidable phenomenon. However, if the fundamental issues related to the behavior of the surface oxides as protective layers are similar to those being addressed for steam-cycle fossil energy plants, the wall thickness of tubing in a steam generator is an order of magnitude smaller than for boiler tubes in fossil plants, placing a greater burden on the development of thin protective oxide layers. On the one hand, progressive reduction of heat transfer by growing oxides can lead to tube overheating and eventually failure [345]. On the other hand, spallation (or exfoliation) of oxide particles can result in blocking of tubes, or if transported further, can erode structural materials.

Oxidation of FM steels in steam produces an oxide scale at the steel surface with essentially a double-layer structure. This duplex oxide scale grows evenly and simultaneously at both the oxide/gas and the metal/oxide interfaces, so that the interface between the two layers may be expected to correspond to the original metal surface. Hydrogen produced by the oxidation process in steam has a significant influence on the corrosion mechanism. Oxidation kinetics is globally parabolic. The parabolic rate constant largely depends on the temperature and the alloying elements of steel (see the significant discrepancy in Fig. 16e). Fig. 16 illustrates an oxidation study for using T91 as structural material of straight tube steam generator [346]. T91 samples have grown a surface oxide scale with a three-layer structure:

- a Fe-Cr spinel layer at the steel/oxide interface,
- a magnetite (Fe_3O_4) layer in contact with steam,
- a top layer of hematite, formed by further oxidation of magnetite.

TEM examinations showed that the spinel oxide ($Fe_{3-x}Cr_xO_4$, $0 < x < 2$) is composed of a large quantity of small equiaxed grains with an average stoichiometry $Fe_{2.4}Cr_{0.6}O_4$. Near the base metal, Fe-rich and Cr-rich grains are alternatively observed. This observation supports the fact that the oxidation model proposed in oxygen-saturated LBE (see section 6.1 [341]) can successfully be applied to oxidation in steam. Oxygen is proposed to be transported to the metal/spinel interface in a molecular form (water molecule). The anionic growth of the internal scale is controlled by the space made available by the metal loss due to formation of the external magnetite scale by cationic flux. The parabolic rate constant from this study was compared to literature data in Fig. 16e.

The SCW reactor (SCWR) design offers higher thermal efficiency and plant simplification as compared to current light water reactors (LWRs). Reactor operating conditions call for a core coolant temperature between 280 °C and 620 °C at a pressure of 25 MPa above the thermodynamical critical point of water (374 °C, 22.1 MPa). The reader is referred to Refs. [65,347] for a detailed review of corrosion issues and stress corrosion cracking in SCWRs. As with traditional light water reactors, environmental degradation in the form of corrosion and stress-corrosion cracking (SCC) are areas of concern, with the nonpolarity of SCW, its radiolysis products, and the higher operating temperatures being possible exacerbating factors. Indeed, SCW exhibits properties significantly different from those of liquid water. It acts like a dense gas and its density can vary with temperature and pressure. Supercritical water will, at the high reactor outlet temperatures, fall in the lower end of the density scale at around 0.2 g/cm^2 while having higher density at the reactor

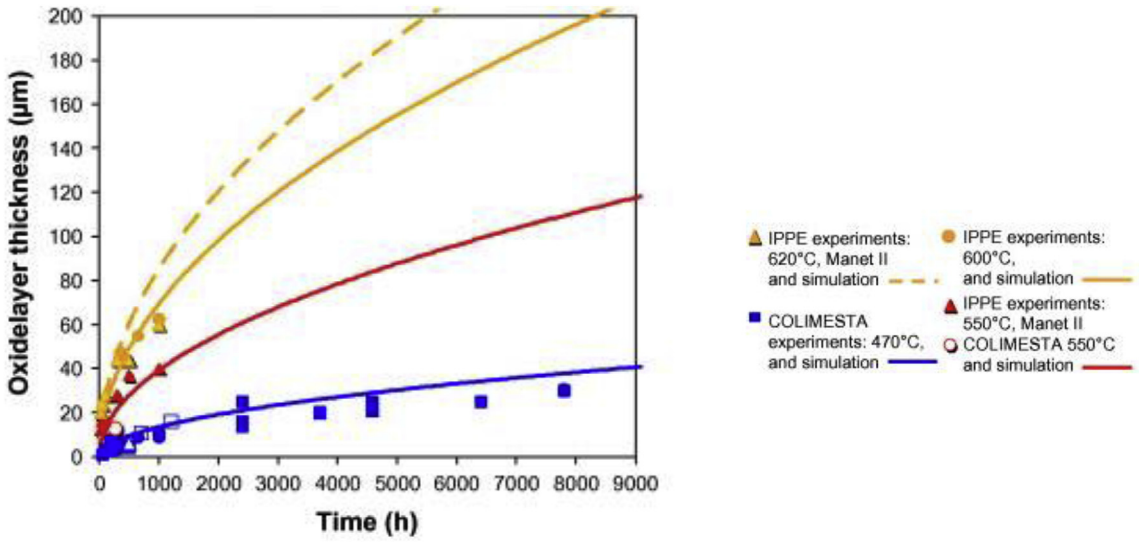

Fig. 15. Oxidation kinetics of T91 steel immersed in oxygen-saturated static Pb-Bi at 470 °C, 550 °C, 600 °C and 620 °C – experimental data and simulations from the Martinelli-Balbaud model [338].

inlet. The corrosivity of SCW over this range of densities varies widely depending upon parameters such as ion product, heat capacity and dielectric constant. At low density (high temperature), SCW is a non-polar solvent of high diffusivity and excellent transport properties. Depending upon what species are present and how much oxygen is dissolved in the solution, SCW in this state can become a very aggressive oxidizing environment.

As in other high-temperature processes, protection against environmental degradation under SCW conditions depends critically on the formation and long-term stability of surface oxide layers on materials. For FM steels, corrosion resistance is associated with the ability of the Fe- and Cr-based surface oxides to function as permeation barriers to the transport of reactants. With the exception of radiation-assisted degradation, the fundamental issues related to the behavior of these oxides as protective layers are similar to those being addressed for advanced steam-cycle fossil energy plants (645 supercritical units and 165 ultra-supercritical units operational worldwide in 2013). However, some consequences of the thickening and failure of these oxides are of concern for thin critical core components such as Fuel Assembly cladding and thin coolant tubes. Although, in general, the detailed oxide growth rate, structure and composition, are specific to the oxygen content of the fluid, temperature, and steel composition, and possibly other factors, the surface oxides are the same in SCW as those typically formed in other oxidizing environments, such as steam (see Fig. 16) and oxygen containing lead alloys.

Much like what is observed under steam conditions for FM steels, the surface scale after immersion in SCW with low dissolved oxygen at 500–600 °C consists of a double-layer structure with an outer magnetite layer and an inner Fe-Cr spinel layer [65,348]. Depending on the steel, a more or less intense internal oxidation zone was observed. High Cr FM steels have corrosion rates significantly higher than austenitic steels. The weight gain from oxidation increases strongly as temperature increases and corrosion resistance increases with increasing Cr content [348]. The influence of dissolved oxygen has been investigated. With a small amount of oxygen, corrosion rates decreased but further addition of dissolved oxygen led to an increase in corrosion rates [347].

Resistance to Stress Corrosion Cracking is the highest challenge for steels in the SCW environment. Stress corrosion studies for SCWR consist mainly in material screening based on slow strain rate tensile tests or constant load experiments. Teysseyre [347] noted that the body of data is large and diverse and difficult to interpret. However, a major conclusion can be drawn: whereas austenitic steels are more corrosion resistant than FM steels (which have substantially lower Cr contents), they are susceptible to SCC in SCW, whereas most of the ferritic and FM alloys are not. The FM were tested in pure SCW in temperature ranging from 370° to 600 °C with various dissolved oxygen content. Only HT9 showed susceptibility to SCC (and this was low). For HT9, crack depth and crack density increase with temperature (400–600 °C) and dissolved oxygen content (up to 300 wppb) [349].

Radiation effects on IGSCC propensity needs to be investigated for SCW conditions. HT9 has been irradiated with 2 MeV protons at 400° and 500 °C to a dose of 7 dpa and tested in pure, deaerated SCW [350]. Cracking increased with irradiation and the authors proposed a correlation with enhanced coarsening of grain boundary carbides.

6.3. Environment effects in gasses

For high temperatures, helium is an excellent heat-transfer gas, because it has a reasonably good thermal conductivity and undergoes no phase transitions. This simplifies the system engineering/design and can be inherently safer. The (very) high temperature reactor is a helium-cooled reactor that will use a compact heat exchanger for power conversion with a gas system or direct cycle on the longer run. Helium outlet temperatures up to 950 °C, possibly 1000 °C, have been envisioned for VHTR. HTR and GFR target a maximum helium at 750° to 850 °C. Modified 9Cr steel was adopted as a highly creep resistant material for reactor pressure vessel (RPV) and/or in core internals in VHTR variants with no cooling of the vessel (RPV temperature above 440 °C).

The helium used as the VHTR cooling gas will invariably have traces of hydrogen, carbon oxides, methane, di-nitrogen … and water vapour. The impurity content may be estimated based on the gas analyses that were performed in experimental helium-cooled reactors [351]: few tens to few hundreds of vppm are expected for H_2, CO, CO_2, CH_4, and N_2, and few tenths of vppm for water vapor content. Such a medium is reactive toward metallic materials at high temperature. However, at sufficiently high oxidizing potentials, the formation of a continuous, dense, slow-growing

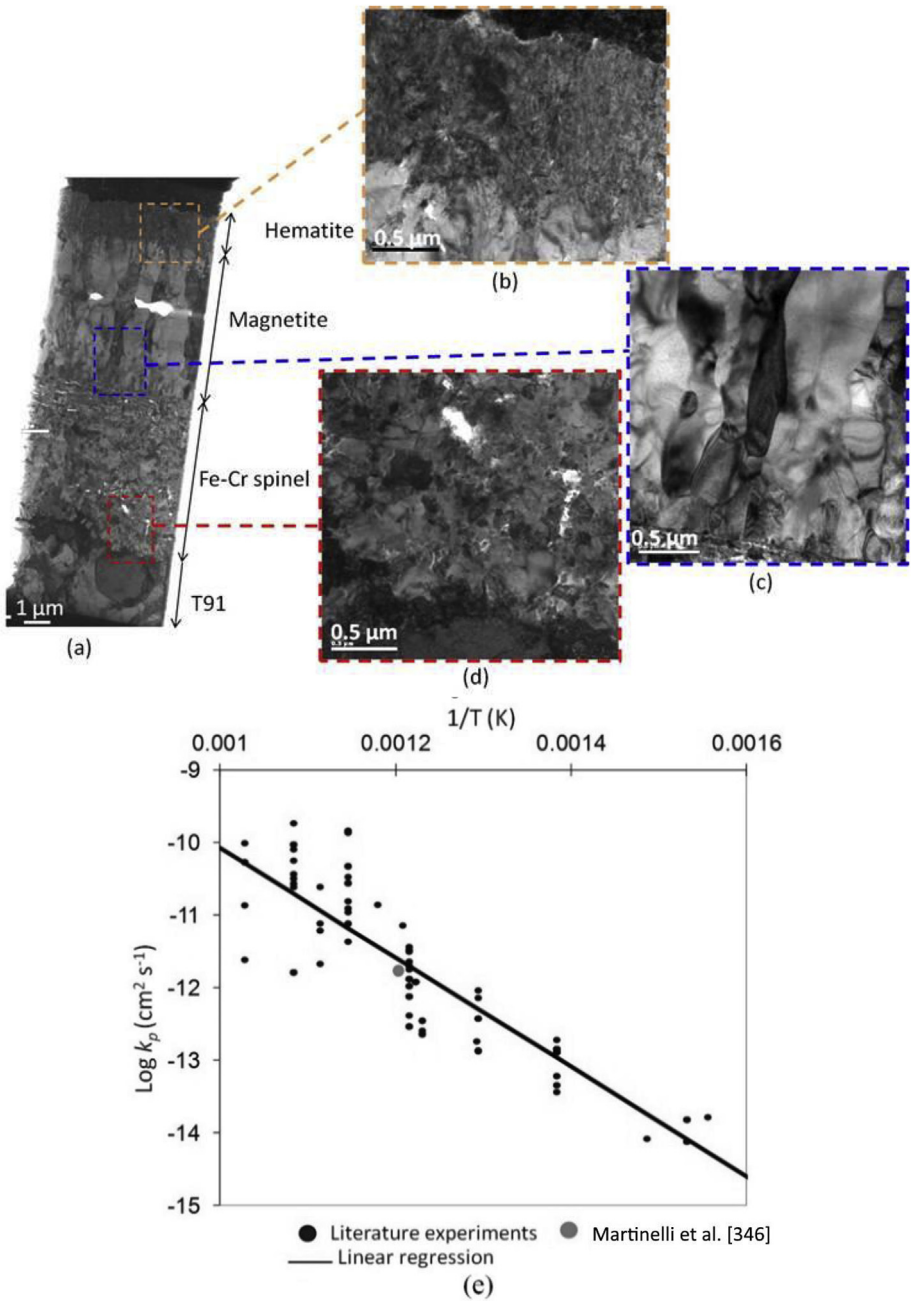

Fig. 16. Oxidation of T91 steel in pure steam at 550 °C. a) cross-section TEM examination of the oxide scale after 48 h), b) zoom on the hematite layer, c) zoom on the magnetite layer, d) zoom on the Fe-Cr spinel layer and e) parabolic rate constant as a function of temperature [346].

surface oxide can act as a barrier against reaction with the reactive species as was discussed for oxidation in steam, in SCW and even in oxygen-saturated LBE.

Few studies that examined the effects of helium with appropriate chemistry —controlled impurity concentrations— on the corrosion of FM steels have been published. Graham [352] reported that surface Cr_2O_3 scales of approximately 2.5 µm are typically formed over a period of 10000 h at 600 °C. With the knowledge gained form the corrosion behaviour of low Cr steels in VHTR helium, decarburization of FM steels should be verified at the highest temperatures when the chromia surface scale may not be protective and internal carbides may react with water vapour leading to a loss of carbon.

Since the end of the 2000s, an increasing interest has been demonstrated on a Brayton cycle working with supercritical CO_2 (SC-CO_2) as new energy conversion systems for various power plants such as solar plants, fossil power plants and nuclear plants like SFR; in such systems, SC-CO_2 would be used at a maximum temperature around 520 °C. Corrosion resistance in SC-CO_2 is one of the important criteria. The corrosion of steels in high temperature CO_2 was studied extensively from the 60's to the 80's in the framework of the development of CO_2-cooled nuclear reactors in France and in the UK. More recent studies have been carried out on the corrosion behavior of steels in extreme conditions for the SC-CO_2 environment in support to the Brayton cycle [46]. In contact with SC-CO_2 at temperatures above 400 °C, 9-12Cr FM steels suffer from two simultaneous corrosion phenomena: oxidation and carburization. The surface oxide scale has a double-layered

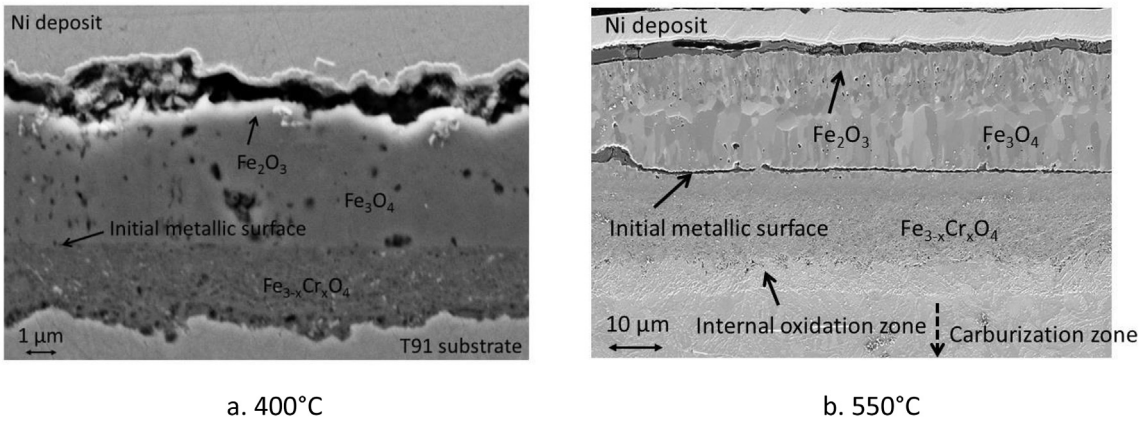

Fig. 17. Cross-section SEM examination of T91 after exposure in flowing SC-CO_2 at 250 bar for 1000 h: a) at 400 °C and b) at 550 °C.

structure, identical to those formed in oxygen-saturated LBE or steam, made of an outer magnetite/hematite layer and an almost-as-thick inner Fe-Cr spinel oxide layer as shown in Fig. 17.

Below the scale, Cr rich carbides were formed and their density and penetration depth increased with time and temperature. GDOES analyses revealed strong carbon transfer to the inner oxide scale and to the T91 substrate at 550 °C but almost none into the substrate at 400 °C.

Exposures of FM steels under CO_2 in the temperature range 400 °C–600 °C and the pressure range 100 bar–200 bar demonstrated that the duplex oxide layer as well as the carburization depth grew according to a parabolic law, at least up to 8000 h [353]. The evolution of the parabolic constant for oxidation as a function of temperature is shown in Fig. 18 and can be written as follows:

$$k_p^{oxidation} = k_p^0 \exp\left(\frac{-E}{RT}\right)$$

with $k_p^0 = 2.97\,10^7$ g^2 m^{-4} h^{-1} and $E = 114$ kJ/mol.

The corrosion mechanistic model, called "Available Space Model" and proposed previously for oxygen containing lead alloys [341] and steam was adapted to SC-CO_2 [353]. This mechanism provides a sound explanation for the simultaneous growth of a duplex oxide and carburization below the oxide scale. The metal consumption and the thickness of the carburized zone were extrapolated from the parabolic laws shown in Fig. 18 and developed in Ref. [353] for the SC-CO_2 IHX outlet temperature of 515 °C and inlet temperature of 340 °C. After 20 years, the metal would have lost only about 0.2 mm but the metal would have been carburized over more than 2 mm. Such a heavy carburization precludes the use of FM steels for the high temperature part of the cycle. However, their use is promising for the low temperature parts with a predicted metal loss of less than 0.1 mm after 20 years at 340 °C.

9-12Cr FM steels were shown to be sensitive to "breakaway" corrosion [46]. Such catastrophic failure of the protective oxide with massive corrosion of the steel occurred at a high CO_2 pressure and high temperature. It was observed that the incubation time prior to rapid steel wastage could be delayed and the post breakaway corrosion rate could be decreased by adding silicon or sulphur in 9-12Cr FM steels and by lowering the water content in SC-CO_2. The mechanism involved in such a breakaway corrosion is still unknown.

Researches have been launched for improving the corrosion resistance of 9-12Cr FM steels and allowing their use at higher temperatures: optimization by alloying element addition, pre-

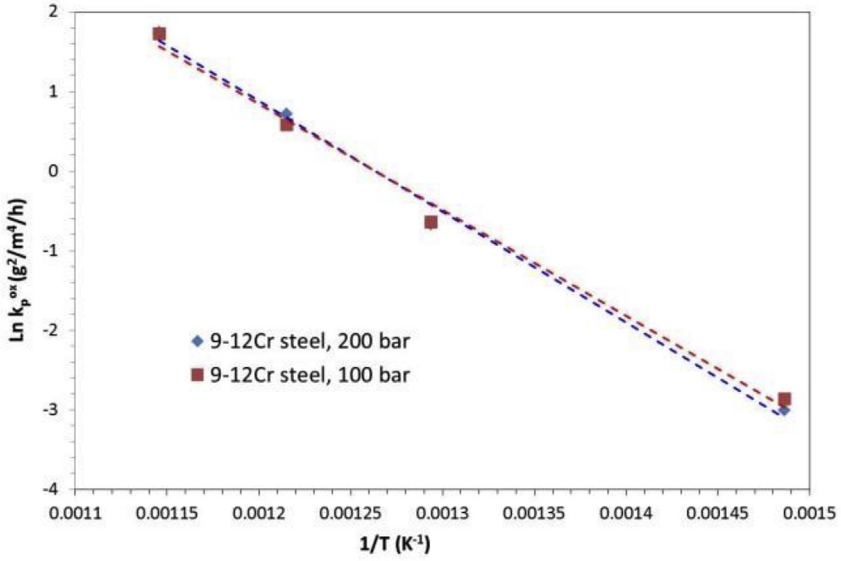

Fig. 18. Parabolic rate constant for 9-12Cr FM steels under high pressure CO_2 in the temperature range 400–600 °C [353].

oxidation treatment or coatings [354].

7. Conclusions

Largely absent from the first operating nuclear reactors in the 1950s and 1960s, FM steels have found numerous nuclear applications since the 1970s, first as core materials for sodium cooled fast reactors, then as structural materials for instance for steam generators. They are now envisaged to be used as core and out-of-core materials in different GEN IV concepts, including as pressure vessel steel for future gas-cooled reactors, and are also considered for fusion applications, in particular in the breeding blankets, as well as for other advanced reactor systems, such as ADS and the TWR.

While they were first selected for core applications mostly due to their superior swelling behavior resulting from a long incubation period, FM steels have other attractive properties among which resistance to high temperature helium embrittlement as well as favorable thermomechanical properties, in particular good resistance to thermal stress development. This later feature is a key reason for which FM steels have been used for steam generator components and are also considered for use in future reactors as piping materials for primary and secondary circuits, allowing compact circuit designs.

Fabrication processes of various product forms, including thick products, are well mastered at industrial scale. Furthermore, high purity several-ton heats of RAFM steels have been produced in different countries using state-of-the-art steelmaking technologies. However further reduction of impurity levels is needed to reach the goal of “hands-on” surface dose rate after an appropriate cooling time, which seems to be technically feasible.

While welding of FM steels is not as straightforward as in the case of stainless steels, due to the need to perform post-weld heat treatments, adequate joining techniques are available and have been thoroughly investigated. Nevertheless, the fabrication of components with complex geometries such as breeding blankets is challenging, and a lot of effort goes into developing appropriate joining strategies and methods.

In view of the very long operating time foreseen for non-replaceable components in future GEN IV reactor designs, the prediction of long-term creep and creep fatigue properties is required. This is very challenging in particular due to the cyclic softening of FM steels, which may for instance drastically lower the creep resistance after cyclic loading, with possible synergistic environmental effects. Existing micro-mechanical models of creep and fatigue behavior should be further developed, as they would help to extrapolate experimental data to the actual in-reactors loading conditions and to better take into account creep fatigue interaction effects in design rules.

In addition to their excellent swelling resistance, after high irradiation doses in a fission environment at temperatures above approximately 400 °C, FM steels show very little hardening and retain a high fracture toughness. Furthermore, the irradiation creep properties of FM steels have been found to be comparable or better than those of austenitic stainless steels. Perhaps the main concern regarding the use of FM for highly irradiated components operating at low temperatures is the irradiation induced embrittlement and degradation of impact and toughness properties occurring in FM steels at temperatures below 400 °C. The issue is particularly critical for the application of FM steels in fusion reactors, since, while the hardening and embrittlement is observed to saturate under fission neutron irradiation, this may not be the case under fusion conditions as the synergistic effects of displacement damage and helium production are not sufficiently understood. Characterization of RAFM steels under fusion relevant neutron spectrum is mandatory in order to properly assess the helium effects and their impact on the lifetime of in-vessel components.

Environmental effects must also be taken into account including possible synergies with irradiation. The Liquid metal embrittlement phenomenon of FM steels by lead alloys, which was found to be enhanced by irradiation hardening, is a good example. The ongoing development of adequate coatings or surface alloying treatments is a promising attempt to mitigate the deleterious effects of aggressive coolants such as lead alloys or high temperature gases on the mechanical properties of FM steels.

Furthermore, the generation of FM steels available in the 70s when they were selected as fast reactor core materials had limited thermal creep resistance. The development of T91 by ORNL at the end of the 70s, initially as part of the fast breader reactor program in the US, was a successful first step in the improvement of the high temperature creep properties of FM steels, as demonstrated by the subsequent widespread use of this steel in the fossil fired and petrochemical industries. While the present baseline RAFM steels exhibit high temperature creep properties slightly inferior to those of T91, efforts to develop RAFM steels with increased high temperature strength and creep performance using adequate TMT and optimized chemical compositions designed with the systematic use of computational thermodynamics have shown promising results, and increasing the operating temperature up to about 600–650 °C seems realistic. In order to further push the limit towards even higher temperature, Oxide Dispersion Strengthened (ODS) ferritic or martensitic steels, produced by powder metallurgy processes, have been designed. They contain high densities of nano-sized particles that act as sinks for point defects and thus dramatically increase the radiation resistance. The nano-oxide interfaces were also shown to trap gasses in the form of small bubbles, thereby mitigating embrittlement effects due to helium. With these outstanding properties, advanced ODS steels are promising materials for use in a fusion environment.

Acknowledgement

Part of this work has been carried out within the framework of the EUROfusion Consortium and has received funding from the Euratom research and training programme 2014–2018 and 2019–2020 under grant agreement No 633053. The views and opinions expressed herein do not necessarily reflect those of the European Commission.

References

[1] Outline history of nuclear energy. http://www.world-nuclear.org/information-library/current-and-future-generation/outline-history-of-nuclear-energy.aspx.
[2] The history of nuclear energy, DOE/NE-0088, U.S. Department of Energy, Office of Nuclear Energy, Science and Technology, Washington, D.C. 20585 https://www.energy.gov/sites/prod/files/The%20History%20of%20Nuclear%20Energy_0.pdf.
[3] Marcoule : G1, G2 and G3 Reactors for Plutonium Production, CEA, 2009. http://fissilematerials.org/library/cea10c.pdf.
[4] Nuclear Power Demonstration Reactor 1962 - 1987, Canadian nuclear society, https://www.cns-snc.ca/media/history/npd/npd.html.
[5] A. Zrodnikov, V. Poplavsky, Y. Ashurko, O. Saraev, N. Oshkanov, M. Bakanov, B. Vasilyev, Y. Kamanin, V. Ershov, M. Svyatkin, A. Korolkov, Y. Krasheninnikov, V. Denisov, Experience gained in Russia on sodium cooled fast reactors and prospects of their further development, in: International Conference on Fast Reactors and Related Fuel Cycles (FR09): Challenges and Opportunities. Kyoto, Japan, December 7-11, 2009 (Book of extended synopses).
[6] Dounreay Fast Reactor celebrates fifty years, Nucl. Eng. Int. (2009). http://www.neimagazine.com/news/newsdounreay-fast-reactor-celebrates-fifty-years.
[7] F. Masuyama, Book, in: Ramaswamy Viswanathan, Jack Nutting (Eds.), Advanced Heat Resistant Steels for Power Generation, 708, The Institute of Materials, 1999, p. 33.

[8] J. Orr, S.J. Sanderson, in: J.W. Davis, D.J. Michel (Eds.), Topical Conference on Ferritic Alloys for Use in Nuclear Energy Technologies, The Metallurgical Society of AIME, Warrendale PA, 1984, p. 261.
[9] C. Cawthorne, E. Fulton, Nature 216 (1967) 575.
[10] J. Bishop, in: Dimensional Stability and Mechanical Behaviour of Irradiated Metals and Alloys, 2, British Nuclear Energy Society, London, 1984, p. 115.
[11] J. Bennett, K. Horton, Metall. Trans A 9 (1978) 143.
[12] D. Harries, J. Standring, W. Barnes, G. Lloyd, in: H. Brager, J. Perrin (Eds.), Effects of Radiation on Materials: Eleventh Conference, ASTM STP 782, American Society for Testing and Materials, Philadelphia PA, 1982, p. 1197.
[13] E. Little, D. Stow, J. Nucl. Mater. 87 (1979) 25.
[14] S. Nomura, S. Shikakura, S. Ukai, I. Seshimo, M. Harada, I. Shibahara, M. Katsuragawa, in: Proceedings of the International Conference on Fast Reactors and Related Fuel Cycles, FR'91, Kyoto, Japan, 1, 1991. Paper 7.4.
[15] A. Uehira, S. Ukai, T. Mizuno, T. Asaga, E. Yoshida, J. Nucl. Sci. Technol. 37 (2000) 780.
[16] K. Anderko, J. Nucl. Mater. 95 (1980) 31.
[17] K. Anderko, J. Nucl. Mater. 95 (1980) 31.
[18] C. Brown, V. Levy, J.-L. Séran, K. Ehrlich, R. Roger, H. Bergmann, in: Proceedings of the International Conference on Fast Reactors and Related Fuel Cycles, FR'91, Kyoto, Japan, 1, 1991. Paper 7.5.
[19] K. Anderko, K. David, W. Ohly, M. Schirra, C. Wassilew, in: J. Davis, D. Michel (Eds.), Proceedings of the Topical Conference on Ferritic Alloys for Use in Nuclear Energy Technologies, The Metallurgical Society of AIME, Warrendale PA, 1984, p. 299.
[20] V. Poplavsky, L. Zabudko, in: Proceedings of the Technical Committee Meeting on: Influence of High Dose Irradiation on Advanced Reactor Core Structural and Fuel Materials, Vienna, Austria, 1998, p. 7. IAEA-TECDOC-1039.
[21] V. Khabarov, A. Dvoriashin, S. Porollo, in: Proceedings of the Technical Committee Meeting on: Influence of High Dose Irradiation on Advanced Reactor Core Structural and Fuel Materials, Vienna, Austria, 1998, p. 139. IAEA-TECDOC-1039.
[22] A.V. Tselishchev, V.S. Ageev, Yu P. Budanov, A.G. Ioltukhovskii, N.M. Mitrofanova, M.V. Leontieva-Smirnova, I.A. Shkabura, L.M. Zabud'ko, A.V. Kozlov, V.V. Mal'tsev, A.V. Povstyanko, Atom. Energy 108 (2010) 274.
[23] A. Lovell, A. Fox, W. Sutherland, S. Hecht, in: Proceedings of the International Conference on Reliable Fuels for Liquid Metal Reactors, American Nuclear Society, LaGrange Park IL, 1987, p. 3.
[24] R. Viswanathan, Adv. Mater. Process. 162 (2004) 73.
[25] B.H. Sencer, J.R. Kennedy, J.I. Cole, S.A. Maloy, F.A. Garner, Microstructural analysis of an HT9 fuel assembly duct irradiated in FFTF to 155 dpa at 443 °C, J. Nucl. Mater. 393 (2009) 235–241.
[26] P. Gavoille, A. Courcelle, J.-L. Séran, X. Averty, B. Bourdiliau, O. Provitina, V. Garat, D. Verwaerde, in: Proceedings of the International Conference on Fast Reactors and Related Fuel Cycles: Safe Technologies and Sustainable Scenarios, FR13, Paris, France, 2013. Paper T4.2.
[27] A. Nikitina, V. Ageev, M. Leont'eva-Smirnova, N. Mitrofanova, I. Naumenko, A. Tselishchev, V. Chernov, Atom. Energy 119 (2016) 362.
[28] U.S. DOE Nuclear Energy Research Advisory Committee, Generation IV International Forum. A Technology Roadmap for Generation IV Nuclear Energy Systems, U.S. DOE Nuclear Energy Research Advisory Committee, Generation IV International Forum, USA, 2002. Report GIF-002-00.
[29] C. Fazio, P. Dubuisson, in: Proceedings of the International Conference on Fast Reactors and Related Fuel Cycles: Safe Technologies and Sustainable Scenarios, FR13, Paris, France, 1, 2013, p. 487.
[30] T. Asayama, Y. Nagae, T. Wakai, M. Inoue, T. Kaito, S. Otuka, N. Kawasaki, M. Morishita, in: International Conference on Fast Reactors and Related Fuel Cycles (FR09) Kyoto, Japan, December 7-11, 2009. https://inis.iaea.org/collection/NCLCollectionStore/_P.
[31] B. Vasilyev, D. Zverev, V. Yershov, S. Kalyakin, V. Poplavskiy, V. Rachkov, O. Sarayev, in: Proceedings of the International Conference on Fast Reactors and Related Fuel Cycles: Safe Technologies and Sustainable Scenarios, FR13, Paris, France, 2013, p. 2.
[32] D. Zhang, in: 49th Meeting of the Technical Working Group on Fast Reactors (TWG-FR), Buenos Aires, Argentina, 2016.
[33] J. Yoo, in: Technical Meeting on Fast Reactors and Related Fuel Cycle Facilities with Improved Characteristics, IAEA, Vienna, Austria, 2013.
[34] P. Patriarca, in: J.W. Davis, D.J. Michel (Eds.), Topical Conference on Ferritic Alloys for Use in Nuclear Energy Technologies, The Metallurgical Society of AIME, Warrendale PA, 1984, p. 107.
[35] C. Willby, J. Walters, in: S. Pugh, E. Little (Eds.), Proceedings of the International Conference on Ferritic Steels for Fast Reactor Steam Generators, 1, British Nuclear Energy Society, London, 1978, p. 40.
[36] R. Anderson, O. Hayden, in: Proceedings of the IAEA-IWGFR Specialists' Meeting on Maintenance and Repair of LMFBR Steam Generators, Oarai, Japan, 1984, p. 185.
[37] G. Kirkland, E. Davies, M. Lambert, Nucl. Technol. 55 (1981) 470.
[38] R. Hosbons, in: J. Davis, D. Michel (Eds.), Proceedings of the Topical Conference on Ferritic Alloys for Use in Nuclear Energy Technologies, The Metallurgical Society of AIME, Warrendale PA, 1984, p. 91.
[39] V. Sikka, C. Ward, K. Thomas, in: Ferritic Steels for High-Temperature Applications : Proceedings of an ASM International Conference on Production, Fabrication, Properties, and Application of Ferritic Steels for High-Temperature Applications, A. Khare Ed..
[40] G. Bodine, R. McDonald, in: A. Khare (Ed.), Ferritic Steels for High-Temperature Applications : Proceedings of an ASM International Conference on Production, Fabrication, Properties, and Application of Ferritic Steels for High-Temperature Applications, American Society for Metals, Metals Park, Ohio, 1983, p. 65.
[41] G. Cunningham, P. Patriarca, E. Hoffman, in: Ferritic Steels for High-Temperature Applications : Proceedings of an ASM International Conference on Production, Fabrication, Properties, and Application of Ferritic Steels for High-Temperature Applications, American Society for Metals, Metals Park, Ohio, 1983, p. 3.
[42] B. Roberts, R. Swindeman, in: K. Coleman (Ed.), Proceedings of the EPRI Conference on 9Cr Materials Fabrication and Joining Technologies, EPRI, Palo Alto, CA, 2001 paper 20-1.
[43] R. Swindeman, M. Santella, P. Maziasz, B. Roberts, K. Coleman, Int. J. Press. Vessel. Pip. 81 (2004) 507.
[44] C. Coussement, in: K. Coleman (Ed.), Proceedings of the EPRI Conference on 9Cr Materials Fabrication and Joining Technologies, EPRI, Palo Alto, CA, 2001, p. 19.
[45] S. Dubiez-Legoff, S. Garnier, O. Gélineau, F. Dalle, M. Blat-Yrieix, J.M. Augem, in: Proceedings of ICAPP'12, Int. Congress on the Advances in Nuclear Power Plants, Chicago, USA, 2012. Paper 12053.
[46] C. Cabet, F. Rouillard, Structural materials for generation IV nuclear reactors, in: P. Yvon (Ed.), Woodhead Publishing Series in Energy Number, 106, 2017, p. 75.
[47] S.C. Chetal, P. Chellapandi, P. Puthiyavinayagam, S. Raghupathy, V. Balasubramaniyan, P. Selvaraj, P. Mohanakrishnan, Baldev Raj, Energy Procedia 7 (2011) 64.
[48] K. Aoto, N. Uto, Y. Sakamoto, T. Ito, M. Toda, S. Kotake, J. Nucl. Sci. Technol. 48 (2011) 463.
[49] Y. Chikazawa, K. Aoto, H. Hayafune, S. Kotake, Y. Ohno, T. Ito, M. Toda, Nucl. Technol. 179 (2012) 360.
[50] https://www.gen-4.org/gif/jcms/c_42149/lead-cooled-fast-reactor-lfr.
[51] G. Bauer, M. Salvatores, G. Heusener, J. Nucl. Mater. 296 (2001) 14.
[52] F. Bianchi, C. Artioli, K. Burn, G. Gherardi, S. Monti, L. Mansani, L. Cinotti, D. Struwe, M. Schikorr, W. Maschek, H. Aït Abderrahim, D. De Bruyn, G. Rimpault, Energy Convers. Manag. 47 (2006) 2698.
[53] Y. Dai, J. Henry, T. Auger, J.-B. Vogt, A. Almazouzi, H. Glasbrenner, F. Groeschel, J. Nucl. Mater. 356 (2006) 308.
[54] W. Wagner, F. Gröschel, K. Thomsen, H. Heyck, J. Nucl. Mater. 377 (2008) 12.
[55] A. Alemberti, J. Carlsson, E. Malambu, A. Orden, D. Struwe, P. Agostini, S. Monti, Nucl. Eng. Des. 241 (2011) 3470.
[56] A. Alemberti, in: Proceedings of the International Workshop on Innovative Nuclear Reactors Cooled by Heavy Liquid Metals: Status and Perspectives, Pisa, Italy, 2012.
[57] A. Alemberti, V. Smirnov, C. Smith, M. Takahashi, Prog. Nucl. Energy 77 (2014) 307.
[58] H. Abderrahim, P. Baeten, D. Bruyn, R. Fernandez, Energy Convers. Manag. 63 (2012) 4.
[59] P. Schuurmans, in: Technical Meeting on Liquid Metal Reactor Concepts: Core Design and Structural Materials, Jun 2013, pp. 12–14. Vienna (Austria).
[60] G. Zelenskii, Yu Ivanov, A. Ioltukhovskii, M. Leont'eva-Smirnova, I. Naumenko, I. Shkabura, Atom. Energy 104 (2008) 120.
[61] Handbook on Lead-bismuth Eutectic Alloy and Lead Properties, Materials Compatibility, Thermal-hydraulics and Technologies 2015 Edition, OECD-NEA, 2015, p. 487. https://www.oecd-nea.org/science/pubs/2015/7268-lead-bismuth-2015.pdf.
[62] A. Weisenburger, A. Heinzel, G. Müller, H. Muscher, A. Rousanov, J. Nucl. Mater. 379 (2008) 274.
[63] M. Konstantinović, E. Stergar, M. Lambrecht, S. Gavrilov, J. Nucl. Mater. 468 (2016) 228.
[64] F. Carre, P. Yvon, P. Anzieu, N. Chauvin, J.-Y. Malo, Nucl. Eng. Des. 240 (2010) 2401.
[65] G. Was, P. Ampornrat, G. Gupta, S. Teysseyre, E. West, T. Allen, K. Sridharan, L. Tan, Y. Chen, X. Ren, C. Pister, J. Nucl. Mater. 371 (2007) 176.
[66] C. Sun, R. Hui, W. Qu, S. Yick, Corros. Sci. 51 (2009) 2508.
[67] P. Hejzlar, et al., Nucl. Eng. Tech. 45 (2013) 731.
[68] G. Was, Z. Jiao, E. Getto, K. Sun, A. Monterrosa, S. Maloy, O. Anderoglu, B. Sencer, M. Hackett, Scripta Mater. 88 (2014) 33.
[69] V. Bryk, O. Borodin, A. Kalchenko, V. Voyevodin, V. Ageev, A. Nikitina, V. Novikov, V. Inozemtsev, A. Zeman, F. Garner, in: Proceedings of the 11th International Topical Meeting on Nuclear Applications of Accelerators, AccApp, Bruges, Belgium, 2013, 2013.
[70] J. Wharry, G. Was, J. Nucl. Mater. 442 (2013) 7.
[71] J. Gigax, T. Chen, H. Kim, J. Wang, L. Price, E. Aydogan, S. Maloy, D. Schreiber, M. Toloczko, F. Garner, L. Shao, J. Nucl. Mater. 482 (2016) 257.
[72] E. Getto, G. Vancoevering, G. Was, J. Nucl. Mater. 484 (2017) 193.
[73] A. Fraas, Nucl. Technol. 22 (1974) 10.
[74] C. McHargue, J. Scott, Met. Trans. A 9A (1978) 151.
[75] M. Williams, R. Santoro, T. Gabriel, Nucl. Technol. 29 (1976) 384.
[76] D. Steiner, Nucl. Fusion 14 (1974) 33.
[77] E. Bloom, J. Nucl. Mater. 85–86 (1979) 795.
[78] T. Lechtenberg, C. Dahms, H. Attaya, in: J. Davis, D. Michel (Eds.), Proceedings of the Topical Conference on Ferritic Alloys for Use in Nuclear Energy Technologies, The Metallurgical Society of AIME, Warrendale PA, 1984, p. 179.

[79] T. Nakayama, M. Abe, T. Tadokoro, M. Otsuka, J. Nucl. Mater. 271–272 (1999) 491.
[80] T. Takagi, Y. Yoshida, P. Ruatto, L. Boccaccini, Fusion Eng. Des. 41 (1998) 313.
[81] A. Hishinuma, A. Kohyama, R. Klueh, D. Gelles, W. Dietz, K. Ehrlich, J. Nucl. Mater. 193 (1998) 258–263.
[82] S. Rosenwasser, P. Miller, J. Dalessandro, J. Rawls, W. Toffolo, W. Chen, J. Nucl. Mater. 85–86 (1979) 177.
[83] D. Harries, in: J. Davis, D. Michel (Eds.), Proceedings of the Topical Conference on Ferritic Alloys for Use in Nuclear Energy Technologies, The Metallurgical Society of AIME, Warrendale PA, 1984, p. 141.
[84] R. Klueh, J. Vitek, J. Nucl. Mater. 150 (1987) 272.
[85] D. Gilbon, C. Rivera, J. Nucl. Mater. 155–157 (1988) 1268.
[86] K. Farell, E. Lee, in: F. Garner, J. Perrin (Eds.), Effects of Radiation on Materials, 12th International Symposium, ASTM STP 870, Philadelphia PA, 1985, p. 383.
[87] U. Stamm, H. Schroeder, J. Nucl. Mater. 155–157 (1988) 1059.
[88] H. Schroeder, H. Ullmaier, J. Nucl. Mater. 179–181 (1991) 118.
[89] H. Böhm, H. Hauck, J. Nucl. Mater. 21 (1967) 112.
[90] H. Böhm, H. Hauck, J. Nucl. Mater. 29 (1969) 184.
[91] Y. Dai, G.R. Odette, T. Yamamoto, in: R. Konings (Ed.), Comprehensive Nuclear Materials, Elsevier, 2012, p. 141.
[92] R. Schäublin, J. Henry, Y. Dai, Compt. Rendus Phys. 9 (2008) 389.
[93] D. Harries, J.-M. Dupouy, C. Wu, J. Nucl. Mater. 133–134 (1985) 25.
[94] K. Ehrlich, S. Kelzenberg, H.-D. Röhrig, L. Schäfer, M. Schirra, J. Nucl. Mater. 212–215 (1994) 678.
[95] E. Bloom, R. Conn, J. Davis, R. Gold, R. Little, K. Schultz, D. Smith, F. Wiffen, J. Nucl. Mater. 122 (1984) 17.
[96] F. Wiffen, R. Santoro, in: J. Davis, D. Michel (Eds.), Topical Conference on Ferritic Alloys for Use in Nuclear Energy Technologies, The Metallurgical Society of AIME, Warrendale PA, 1984, p. 195.
[97] F. Mann, J. Nucl. Mater. 123 (1984) 1053.
[98] K. Ehrlich, S. Cierjacks, S. Kelzenberg, A. Möslang, in: D. Gelles, R. Nanstad, A. Kumar, E. Little (Eds.), Effects of Radiation on Materials, 17th International Symposium, ASTM STP 1270, West Conshohocken PA, 1996, p. 1109.
[99] G. Butterworth, L. Giancarli, J. Nucl. Mater. 155–157 (1988) 575.
[100] D. Dulieu, K. Tupholme, G. Butterworth, J. Nucl. Mater. 141–143 (1986) 1097.
[101] K. Tupholme, D. Dulieu, G. Butterworth, J. Nucl. Mater. 155–157 (1988) 650.
[102] M. Tamura, H. Hayakawa, M. Tanimura, A. Hishinuma, T. Kondo, J. Nucl. Mater. 141–143 (1986) 1067.
[103] T. Noda, F. Abe, H. Araki, M. Okada, J. Nucl. Mater. 141–143 (1986) 1102.
[104] A. Kimura, H. Kayano, T. Misawa, H. Matsui, J. Nucl. Mater. 212–215 (1994) 690.
[105] A. Kohyama, Y. Kohno, K. Asakura, H. Kayano, J. Nucl. Mater. 212–215 (1994) 684.
[106] R. Klueh, E. Bloom, Nuclear engineering and design, Fusion 2 (1985) 383.
[107] C.-Y. Hsu, T. Lechtenberg, J. Nucl. Mater. 141–143 (1986) 1107.
[108] R. Klueh, D. Gelles, T. Lechtenberg, J. Nucl. Mater. 141–143 (1986) 1081.
[109] D. Gelles, in: R. Klueh, D. Gelles, M. Okada, N. Packan (Eds.), Reduced Activation Materials for Fusion Reactors, ASTM STP 1047, Philadelphia PA, 1990, p. 113.
[110] N. Yamanouchi, M. Tamura, H. Hayakawa, A. Hishinuma, T. Kondo, J. Nucl. Mater. 191–194 (1992) 822.
[111] A. Kohyama, A. Hishinuma, D. Gelles, R. Klueh, W. Dietz, K. Ehrlich, J. Nucl. Mater. (1996) 233–237, 138.
[112] B. van der Schaaf, D. Gelles, S. Jitsukawa, A. Kimura, R. Klueh, A. Möslang, G. Odette, J. Nucl. Mater. 283–287 (2000) 52.
[113] R. Lindau, A. Möslang, M. Rieth, M. Klimiankou, E. Materna-Morris, A. Alamo, A.-A.F. Tavassoli, C. Cayron, A.-M. Lancha, P. Fernandez, N. Baluc, R. Schäublin, E. Diegele, G. Filacchioni, J.W. Rensman, B. van der Schaaf, E. Lucon, W. Dietz, Fusion Eng. Des. 75–79 (2005) 989.
[114] H. Tanigawa, Y. Someya, H. Sakasegawa, T. Hirose, K. Ochiai, Fusion Eng. Des. 89 (2014) 1573.
[115] Q. Huang, C. Li, Y. Li, M. Chen, M. Zhang, L. Peng, Z. Zhu, Y. Song, S. Gao, J. Nucl. Mater. (2007) 367–370, 142.
[116] Q. Huang, N. Baluc, Y. Dai, S. Jitsukawa, A. Kimura, J. Konys, R. Kurtz, R. Lindau, T. Muroga, G. Odette, B. Raj, R. Stoller, L. Tan, H. Tanigawa, A. Tavassoli, T. Yamamoto, F. Wan, Y. Wu, J. Nucl. Mater. 442 (2013) S2.
[117] S. Raju, B. Ganesh, A. Rai, R. Mythili, S. Saroja, E. Mohandas, M. Vijayalakshmi, K. Rao, B. Raj, J. Nucl. Mater. 389 (2009) 385.
[118] B. Raj, K. Rao, A. Bhaduri, Fusion Eng. Des. 85 (2010) 1460.
[119] Y. Chun, S. Kang, S. Noh, T. Kim, D. Lee, S. Cho, Y. Jeong, J. Nucl. Mater. 455 (2014) 212.
[120] M. Leonteva-Smirnova, A. Ioltukhovskiy, G. Arutiunova, A. Tselischev, V. Chernov, J. Nucl. Mater. 307–311 (2002) 466.
[121] V. Chernov, M. Leonteva-Smirnova, M. Potapenko, N. Budylkin, Yu Devyatko, A. Ioltoukhovskiy, E. Mironova, A. Shikov, A. Sivak, G. Yermolaev, A. Kalashnikov, B. Kuteev, A. Blokhin, N. Loginov, V. Romanov, V. Belyakov, I. Kirillov, T. Bulanova, V. Golovanov, V. Shamardin, Yu Strebkov, A. Tyumentsev, B. Kardashev, O. Mishin, B. Vasiliev, Nucl. Fusion 47 (2007) 839.
[122] H. Tanigawa, E. Gaganidze, T. Hirose, M. Ando, S. Zinkle, R. Lindau, E. Diegele, Nucl. Fusion 57 (2017), 092004.
[123] E. Gaganidze, C. Petersen, E. Materna-Morris, C. Dethloff, O. Weiß, J. Aktaa, A. Povstyanko, A. Fedoseev, O. Makarov, V. Prokhorov, J. Nucl. Mater. 417 (2011) 93.
[124] J. Henry, X. Averty, A. Alamo, J. Nucl. Mater. 417 (2011) 99.
[125] A. Tavassoli, E. Diegele, R. Lindau, N. Luzginova, H. Tanigawa, J. Nucl. Mater. 455 (2014) 269.
[126] M. Zmitko, Y. Carin, N. Thomas, M. Simon-Perret, A. LiPuma, L. Forest, J. Tosi, G. Aiello, L. Cogneau, J. Rey, H. Neuberger, J. Aktaa, E. Gaganidze, K. Zhang, N. Pierredon, Y. Lejeail, P. Lamagnere, Y. Poitevin, Fusion Eng. Des. 124 (2017) 767.
[127] S. Zinkle, J.-L. Boutard, D. Hoelzer, A. Kimura, R. Lindau, G. Odette, M. Rieth, L. Tan, H. Tanigawa, Nucl. Fusion 57 (2017), 092005.
[128] F. Abe, F. Abe F, T. Kern, R. Viswanathan (Eds.), Creep-resistant Steels, Woodhead Publishing, Cambridge, UK, 2008, p. 279.
[129] L. Tan, Y. Yang, J. Busby, J. Nucl. Mater. 442 (2013) S13.
[130] J. Hoffmann, M. Rieth, L. Commin, P. Fernández, M. Roldán, Nucl. Mater. Energy 6 (2016) 12.
[131] L. Tan, L.L. Snead, Y. Katoh, J. Nucl. Mater. 478 (2016) 42.
[132] C. Cristalli, L. Pilloni, O. Tassa, L. Bozzetto, R. Sorci, L. Masotti, Nucl. Mater. Energy 16 (2018) 175.
[133] L. Tan, C. Parish, X. Hu, J. Nucl. Mater. 509 (2018) 267.
[134] L. Tan, Y. Katoh, L. Snead, J. Nucl. Mater. 511 (2018) 598.
[135] R. Klueh, D. Harries, in: High-Chromium Ferritic and Martensitic Steels for Nuclear Applications, ASTM MONO3, American Society for Testing and Materials, West Conshohocken, PA, 2001.
[136] T. Asayama, in: P. Yvon (Ed.), Structural Materials for Generation IV Nuclear Reactors, 2017, p. 635.
[137] P. Bocquet, Ph Bourges, A. Cheviet, Nucl. Eng. Des. 144 (1993) 149.
[138] S. Pillot, Z. Zhao, S. Corre, C. Chauvy, L. Coudreuse, P. Toussaint, in: Proceedings of the ASME 2010 Pressure Vessels & Piping Division, Washington, USA, 2010. Paper PVP2010-25628.
[139] K. Haarmann, J.-C. Vaillant, B. Vandenberghe, W. Bendick, A. Arbab, The T91/P91 Book, Vallourec & Mannesmann Tubes, 1999.
[140] J. Gabrel, W. Bendick, C. Zakine, B. Vandenberghe, in: Proceedings of CREEP8, Eighth International Conference on Creep and Fatigue at Elevated Temperatures, 2007, p. 189. Paper CREEP2007-26571.
[142] Y. Nagae, T. Onizawa, S. Takaya, T. Yamashita, in: Proceedings of the ASME 2014 Pressure Vessels and Piping Conference PVP 2014, California, USA, 2014. Paper PVP2014-28689.
[143] S.A. David, J.A. Siefert, Z. Feng, Sci. Technol. Weld. Join. 18 (2013) 631.
[144] J.C. Lippold, J. Nucl. Mater. 103–104 (1981) 1127.
[145] Y. Yano, T. Kaito, T. Tanno, S. Ohtsuka, J. Nucl. Sci. Technol. 52 (2015) 568.
[146] G. Filacchioni, R. Montanari, M.E. Tata, L. Pilloni, J. Nucl. Mater. 307–311 (2002) 1563.
[147] S. Wu, J. Zhang, J. Yang, J. Lu, H. Liao, X. Wang, J. Nucl. Mater. 503 (2018) 66.
[148] H. Hayakawa, A. Yoshitake, M. Tamura, S. Natsume, A. Gotoh, A. Hishinuma, J. Nucl. Mater. 179–181 (1991) 693.
[149] G. Srinivasan, B. Arivazhagan, S.K. Albert, A.K. Bhaduri, Fusion Eng. Des. 86 (2011) 446.
[150] T. Narita, S. Ukai, T. Kaito, S. Ohtsuka, M. Fujiwara, J. Nucl. Sci. Technol. 42 (2005) 825.
[151] T. Sawai, K. Shiba, A. Hishinuma, J. Nucl. Mater. 283–287 (2000) 657.
[152] M. Zmitko, Y. Carin, N. Thomas, M. Simon-Perret, A. Li Puma, L. Forest, J. Tosi, G. Aiello, L. Cogneau, J. Rey, H. Neuberger, J. Aktaa, E. Gaganidze, K. Zhang, N. Pierredon, Y. Lejeail, P. Lamagnère, Y. Poitevin, Fusion Eng. Des. 124 (2017) 767.
[153] H. Tanigawa, T. Hirose, K. Shiba, R. Kasada, E. Wakai, H. Serizawa, Y. Kawahito, S. Jitsukawa, A. Kimura, Y. Kohno, A. Kohyama, S. Katayama, H. Mori, K. Nishimoto, R.L. Klueh, M.A. Sokolov, R.E. Stoller, S.J. Zinkle, Fusion Eng. Des. 83 (2008) 1471.
[154] G. Aiello, J. Aubert, L. Forest, J.-C. Jaboulay, A. Li Puma, L.V. Boccaccini, Nucl. Fusion 57 (2017), 046022.
[155] K. Sawada, K. Suzuki, H. Kushima, M. Tabuchi, K. Kimura, Mater. Sci. Eng. A 480 (2008) 558.
[156] R.L. Klueh, J. Nucl. Mater. 378 (2008) 159.
[157] F. Abe, Sci. Technol. Adv. Mater. 9 (2008), 013002.
[158] R.L. Klueh, N. Hashimoto, P.J. Maziasz, in: Proceedings of the 21st IEEE/NPSS Symposium on Fusion Engineering SOFE, 05, 2006, p. 287.
[159] S. Hollner, B. Fournier, J. Le Pendu, T. Cozzika, I. Tournié, J.-C. Brachet, A. Pineau, J. Nucl. Mater. 405 (2010) 101.
[160] E. Piozin, PhD Thesis, ISSN 0429-3460, CEA-R-6402 (2015).
[161] S. Hollner, E. Piozin, P. Mayr, C. Caës, I. Tournié, A. Pineau, B. Fournier, J. Nucl. Mater. 441 (2013) 15.
[162] P. Fernandez, J. Hoffmann, M. Rieth, M. Roldan, A. Gomez-Herrero, J. Nucl. Mater. 500 (2018) 1.
[163] R. Lim, F. Dalle, M. Sauzay, L. Allais, I. Tournié, P. Bonnaillie, J. Malaplate, A.F. Gourgues-Lorenzon, in: Proceedings of the 12th Int. Conf. On Creep and Fracture for Engineering Materials and Structure, Kyoto, Japan, 2011.
[164] T. Massé, Y. Lejeail, Nucl. Eng. Des. 246 (2012) 220.
[165] K. Kimura, H. Kushima, F. Abe, K. Yagi, Mater. Sci. Eng. A 234–236 (1997) 1079.
[166] E.M. Haney, F. Dalle, M. Sauzay, L. Vincent, I. Tournié, L. Allais, B. Fournier, Mater. Sci. Eng. A 510–511 (2009) 99.
[167] T. Onizawa, Y. Nagae, S. Takaya, T. Asayama, in: Proceedings of the ASME 2013 Pressure Vessels and Piping Conf. PVP2013, Paris, France, 2013. Paper PVP2013-97611.
[168] K. Kimura, M. Yaguchi, in: Proceedings of the ASME 2016 Pressure Vessels and Piping Conf. PVP 2016, Vancouver, Canada, 2016. Paper PVP2016-63355.
[169] ECCC datasheets. http://eccc.c-s-m.it/, 2017.

[170] B. Founier, M. Salvi, F. Dalle, Y. de Carlan, C. Caës, M. Sauzay, A. Pineau, Int. J. Fatigue 32 (2010) 971.
[171] J.S. Dubey, H. Chilukuru, J.K. Chakravartty, M. Schwienheer, A. Scholz, W. Blum, Mater. Sci. Eng. A 406 (2005) 152.
[172] A.F. Armas, C. Petersen, R. Schmitt, M. Avalos, I. Alvarez, J. Nucl. Mater. 329–333 (2004) 252.
[173] P. Marmy, T. Kruml, J. Nucl. Mater. 377 (2008) 52.
[174] B. Fournier, F. Dalle, M. Sauzay, J. Longour, M. Salvi, C. Caës, I. Tournié, P.-F. Giroux, S.-H. Kim, Mater. Sci. Eng. A 528 (2011) 6934.
[175] M. Sauzay, H. Brillet, I. Monnet, M. Mottot, F. Barcelo, B. Fournier, A. Pineau, Mater. Sci. Eng. A 400–401 (2005) 241.
[176] S. Kim, J.R. Weertman, Metal. Trans. A 19A (1988) 999.
[177] K. Shiba, H. Tanigawa, T. Hirose, H. Sakasegawa, S. Jitsukawa, Fusion Eng. Des. 86 (2011) 2895.
[178] P. Fernandez, M. Garcia-Mazario, A.M. Lancha, J. Lapeña, J. Nucl. Mater. 329–333 (2004) 273.
[179] Y. Yano, T. Tanno, Y. Sekio, H. Oka, S. Ohtsuka, T. Uwabata, T. Kaito, Nuc. Mater. Energy 9 (2016) 324.
[181] R.L. Klueh, K. Shiba, M.A. Sokolov, J. Nucl. Mater. 377 (2008) 427.
[182] H. Tanigawa, K. Shiba, A. Möslang, R.E. Stoller, R. Lindau, M.A. Sokolov, G.R. Odette, R.J. Kurtz, S. Jitsukawa, J. Nucl. Mater. 417 (2011) 9.
[183] S. Kunimitsu, Y. You, N. Kasuya, Y. Sasaki, Y. Hosoi, J. Nucl. Mater. 179–181 (1991) 689.
[184] Y. de Carlan, A. Alamo, M.H. Mathon, G. Geoffroy, A. Castaing, J. Nucl. Mater. 283–287 (2000) 672.
[185] American Society of Mechanical Engineers, Boiler and Pressure Vessel Code .
[186] Japan Society of Mechanical Engineers, Code for Nuclear Power Generation Facilities, Rules on Design and Construction for Nuclear Power Plants .
[187] Association Française pour les règles de conception et de construction des Chaudières Electro-Nucléaires, Design and Construction Rules for Mechanical Component of Nuclear Installations RCC-MRx.
[188] R.J. Kurtz, A. Alamo, E. Lucon, Q. Huang, S. Jitsukawa, A. Kimura, R.L. Klueh, G.R. Odette, C. Petersen, M.A. Sokolov, P. Spätig, J.-W. Rensman, J. Nucl. Mater. 386–388 (2009) 411.
[189] E. Gaganidze, F. Gillemot, I. Szenthe, M. Gorley, M. Rieth, E. Diegele, Fusion Eng. Des. 135 (2018) 9.
[190] M. Zmitko, J. Galabert, N. Thomas, L. Forest, P. Bucci, L. Cogneau, J. Rey, H. Neuberger, Y. Poitevin, Fusion Eng. Des. 96–97 (2015) 199.
[191] R.L. Klueh, A.T. Nelson, J. Nucl. Mater. 371 (2007) 37.
[192] N. Baluc, K. Abe, J.L. Boutard, V.M. Chernov, E. Diegele, S. Jitsukawa, A. Kimura, R.L. Klueh, A. Kohyama, R.J. Kurtz, R. Lässer, H. Matsui, A. Möslang, T. Muroga, G.R. Odette, M.Q. Tran, B. Van der Schaaf, Y. Wu, J. Yu, S.J. Zinkle, Nucl. Fusion 47 (2007).
[193] M. Gorley, E. Diegele, S. Dudarev, G. Pintsuk, Fusion Eng. Des. 136 (2018) 298.
[194] O. Ancelet, M.N. Berton, M. Blat, F. Dalle, P. Dubuisson, O. Gélineau, Y. Lejeail, in: Proceedings of the Int. Conference on Fast Reactors and Related Fuel Cycles FR09, Kyoto, Japan, 2009. Paper 04-08.
[195] E. Gaganidze, J. Aktaa, Fusion Eng. Des. 88 (2013) 118.
[196] H. Tanigawa, E. Gaganidze, T. Hirose, M. Ando, S.J. Zinkle, R. Lindau, E. Diegele, Nucl. Fusion 57 (2017), 092004.
[197] D.S. Gelles, J. Nucl. Mater. 148 (1987) 136.
[198] T. Morimura, A. Kimura, H. Matsuie, J. Nucl. Mater. 239 (1996) 118.
[199] M.B. Toloczko, F.A. Garner, J. Nucl. Mater. 233–237 (1996) 289.
[200] A.M. Dvoriashin, S.I. Porollo, Yu V. Konobeev, F.A. Garner, J. Nucl. Mater. 329–333 (2004) 319.
[201] R. Lindau, A. Möslang, J. Nucl. Mater. 212–215 (1994) 599.
[202] R.L. Klueh, Ji-Jung Kai, D.J. Alexander, J. Nucl. Mater. 225 (1995) 175.
[203] C. Petersen, V. Shamardin, A. Fedoseev, G. Shimansky, V. Efimov, J. Rensman, J. Nucl. Mater. 307–311 (2002) 1655.
[204] H.-C. Schneider, B. Dafferner, J. Aktaa, J. Nucl. Mater. 321 (2003) 135.
[205] E. Lucon, M. Decreton, E. van Walle, Fusion Eng. Des. 69 (2003) 373.
[206] H. Tanigawa, N. Hashimoto, H. Sakasegawa, R.L. Klueh, M.A. Sokolov, K. Shiba, S. Jitsukawa, A. Kohyama, J. Nucl. Mater. 329–333 (2004) 283.
[207] J. Rensman, E. Lucon, J. Boskeljon, J. van Hoepen, R. den Boef, P. ten Pierick, J. Nucl. Mater. 329–333 (2004) 1113.
[208] E. Gaganidze, H.-C. Schneider, B. Dafferner, J. Aktaa, J. Nucl. Mater. 355 (2006) 83.
[209] H. Tanigawa, H. Sakasegawa, N. Hashimoto, R.L. Klueh, M. Ando, M.A. Sokolov, J. Nucl. Mater. 367–370 (2007) 42.
[210] A. Alamo, J.L. Bertin, V.K. Shamardin, P. Wident, J. Nucl. Mater. 367–370 (2007) 54.
[211] C. Petersen, A. Povstyanko, V. Prokhorov, A. Fedoseev, O. Makarov, B. Dafferner, J. Nucl. Mater. 367–370 (2007) 544.
[212] C. Petersen, A. Povstyanko, V. Prokhorov, A. Fedoseev, O. Makarov, M. Walter, J. Nucl. Mater. 386–388 (2009) 299.
[213] E. Materna-Morris, A. Moeslang, R. Rolli, H.-C. Schneider, J. Nucl. Mater. 386–388 (2009) 422.
[215] J. Henry, X. Averty, A. Alamo, J. Nucl. Mater. 417 (2011) 99.
[216] E. Materna-Morris, A. Möslang, R. Rolli, H.-C. Schneider, Fusion Eng. Des. 86 (2011) 2607.
[217] O. Anderoglu, T.S. Byun, M. Toloczko, S.A. Maloy, Metall. Mater. Trans. A 44A (2013) 70.
[218] J. Henry, S.A. Maloy, Structural Materials for Generation IV Nuclear Reactors, 2017, p. 329.
[219] D.S. Gelles, J. Nucl. Mater. 122–123 (1994) 207.
[220] D.S. Gelles, J. Nucl. Mater. 233–237 (1996) 293.
[221] R. Schäublin, M. Victoria, Mater. Res. Soc. Symp. Proc. 650 (2001). R1.8.1.
[222] M.H. Mathon, Y. de Carlan, G. Geoffroy, X. Averty, A. Alamo, C.H. de Novion, J. Nucl. Mater. 312 (2003) 236.
[223] E. Materna-Morris, A. Möslang, H.C. Schneider, R. Rolli, in: Proceedings of 22nd IAEA Fusion Energy Conference, Geneva, Switzerland, 2008, p. 1.
[224] H. Tanigawa, R.L. Klueh, N. Hashimoto, M.A. Sokolov, J. Nucl. Mater. 386–388 (2009) 231.
[225] M. Klimenkov, E. Materna-Morris, A. Moeslang, J. Nucl. Mater. 417 (2011) 124.
[226] O. Weiss, E. Gaganidze, J. Aktaa, J. Nucl. Mater. 426 (2012) 52.
[227] S.V. Rogozhkin, A.A. Nikitin, A.A. Aleev, A.B. Germanov, A.G. Zaluzhnyi, Inorg. Mater.: Applied Research 4 (2013) 112.
[228] L. Tan, B.K. Kim, Y. Yang, K.G. Field, S. Gray, M. Li, J. Nucl. Mater. 493 (2017) 12.
[229] R. Coppola, E. Gaganidze, M. Klimenkov, C. Dethloff, R. Lindau, M. Valli, J. Aktaa, A. Möslang, Nuclear Materials and Energy 9 (2016) 189.
[230] C. Dethloff, E. Gaganidze, J. Aktaa, Nuclear Materials and Energy 9 (2016) 471.
[231] C. Dethloff, E. Gaganidze, J. Aktaa, Nuclear Materials and Energy 15 (2018) 23.
[232] S. Yamashita, Y. Yano, T. Tachi, N. Akasaka, J. Nucl. Mater. 386–388 (2009) 135.
[233] H. Tanigawa, H. Sakasegawa, N. Hashimoto, R.L. Klueh, M. Ando, M.A. Sokolov, J. Nucl. Mater. 367–370 (2007) 42.
[234] H. Tanigawa, N. Hashimoto, H. Sakasegawa, et al., J. Nucl. Mater. 329–333 (2004) 283.
[235] X. Jia, Y. Dai, M. Victoria, J. Nucl. Mater. 305 (2002) 1.
[236] L. Tan, B.K. Kim, Y. Yang, K.G. Field, S. Gray, M. Li, J. Nucl. Mater. 493 (2017) 12.
[237] P. Dubuisson, D. Gilbon, J.L. Seran, J. Nucl. Mater. 205 (1993) 178.
[238] J.J. Kai, R.L. Klueh, J. Nucl. Mater. 230 (1996) 116.
[239] C. Dethloff, E. Gaganidze, J. Aktaa, J. Nucl. Mater. 454 (2014) 323.
[240] J.P. Wharry, G.S. Was, J. Nucl. Mater. 442 (2013) 7.
[241] J. Wharry, G. Was, Acta Mater. 65 (2014) 42.
[242] R.L. Klueh, D.J. Alexander, J. Nucl. Mater. 233–237 (1996) 336.
[243] R.L. Klueh, D.J. Alexander, J. Nucl. Mater. 265 (1999) 262.
[244] R.L. Klueh, D.J. Alexander, J. Nucl. Mater. 218 (1995) 151.
[245] H. Kayano, A. Kimura, M. Narui, Y. Sasaki, Y. Suzuki, S. Ohta, J. Nucl. Mater. 155–157 (1988) 978.
[246] W.L. Hu, D.S. Gelles, Influence of radiation on material properties: 13th international symposium (Part 11), ASTM STP 956 (1987) 83.
[247] R.L. Klueh, J.M. Vitek, W.R. Corwin, D.J. Alexander, J. Nucl. Mater. 155–157 (1988) 973.
[248] T. Lechtenberg, J. Nucl. Mater. 133–134 (1985) 149.
[249] R.L. Klueh, D.J. Alexander, J. Nucl. Mater. 179–181 (1991) 733.
[250] D.S. Gelles, J. Nucl. Mater. 230 (1996) 187.
[251] R.L. Klueh, D.J. Alexander, J. Nucl. Mater. 258–263 (1998) 1269.
[252] R.L. Klueh, D.J. Alexander, in: Proceedings of ICFRM-, 1995, p. 336.
[253] R.L. Klueh, D.J. Alexander, M. Rieth, J. Nucl. Mater. 273 (1999) 146.
[254] R.L. Klueh, M.A. Sokolov, K. Shiba, Y. Miwa, J.P. Robertson, J. Nucl. Mater. 283–287 (2000) 478.
[255] J.L. Seran, A. Alamo, A. Maillard, H. Touron, J.C. Brachet, P. Dubuisson, O. Rabouille, J. Nucl. Mater. 212–215 (1994) 588.
[256] J.W. Rensman, H.E. Hofmans, E.W. Schuring, J. van Hoepen, J.B.M. Bakker, R. den Boef, F.P. van den Broek, E.D.L. van Essen, J. Nucl. Mater. 307–311 (2002) 250.
[257] K. Shiba, A. Hishinuma, A. Toyama, K. Masamura, "Properties of the reduced activation ferritic steel F82H IEA heat (in Japanese)", JAERI-Tech 97-9038.
[258] H.-C. Schneider, B. Dafferner, H. Ries, O. Romer, Bestrahlungsprogramm MANITU, Ergebnisse der Krbschlagbiegeversuche mit den bis 2,4 dpa bestrahlten Werkstoffen, FZKA 6605 (2001).
[259] M.A. Sokolov, "Fracture Toughness Characerization of Irradiated F82H".ASTM.
[260] J. Rensman, J. van Hoepen, J.B.M. Bakker, R. den Boef, F.P. van den Broek, E.D.L. van Essen, J. Nucl. Mater. 307–311 (2002) 245.
[261] M.L. Hamilton, L.E. Schubert, D.S. Gelles, J. Nucl. Mater. 258–263 (1998) 1222.
[262] M. Rieth, B. Dafferner, H.-D. Roehrig, J. Nucl. Mater. 258–263 (1998) 1147.
[263] E.I. Materna-Morris, M. Rieth, K. Ehrlich, in: Effects of Radiation on Materials: 19th International Symposium, 1366, ASTM STP, 2000, p. 597.
[264] E.V. van Osch, J.B.M., Bakker, R. den Boef, J. Rensman.NRG Petten 20023/99.26974/P.
[265] Y. Kohno, A. Kohyama, T. Hirose, M.L. Hamilton, M. Narui, J. Nucl. Mater. 271–272 (1999) 145.
[266] E. van Osch, M. Horsten, G.E. Lucas, G.R. Odette, in: Effect of Radiation on Materials: 19th International Symposium, STP1366, 2000, p. 612.
[267] A. Kimura, M. Narui, T. Misawa, H. Matsui, A. Kohyama, J. Nucl. Mater. 258–263 (1998) 1340.
[268] A. Alamo, M. Horsten, X. Averty, E.I. Materna-Morris, M. Rieth, J.C. Brachet, J. Nucl. Mater. 283–287 (2000) 353.
[269] I. Belianov, P. Marmy, J. Nucl. Mater. 258–263 (1998) 1259.
[270] N. Baluc, R. Schaublin, C. Bailat, F. Paschoud, M. Victoria, J. Nucl. Mater. 283–287 (2000) 731.
[271] R.L. Klueh, D.J. Alexander, in: Effects of Radiation on Materials: 18th

International Symposium, ASTM STP 1325, 1999, p. 911.
[272] H. Tanigawa, K. Shiba, Fusion Sci. Technol. 44 (2003) 206.
[273] Y. Yano, K. Oka, N. Akasaka, T. Yoshitake, Y. Abe, S. Ohnuki, J. Nucl. Sci. Technol. 43 (2006) 648.
[274] C. Petersen, Post Irradiation Examination of RAF/M Steels after Fast Reactor Irradiation up to 33 Dpa and < 340°C (ARBOR 1), EFDA TW2-TTMS-001b D9, Karlsruher Institut für Technologie, 2010. FZKA 7517.
[275] E. Materna-Morris, A. Möslang, H.-C. Schneider, J. Nucl. Mater. 442 (2013) 62.
[277] E.V. van Osch, J.V. van Hoepen, J. Boskeljon, J. Rensman, "Tensile Properties of 2.5 Dpa 300 oC Neutron Irradiatied RA FM Plate, Powder HIP and EB and TIG Weld".NRG Petten 20023/99.26704/P.
[279] E. Materna-Morris, H.-C. Schneider, A. Möslang, „Tensile behavior of RAFM alloys after neutron irradiation of up to 16.3 dpa between 250 and 450°C, J. Nucl. Mater. 455 (2014) 728–734.
[280] Y. Yano, T. Yoshitake, S. Yamashita, N. Akasaka, S. Onose, H. Takahashi, J. Nucl. Mater. 367–370 (2007) 127.
[281] Y. Yano, T. Yoshitake, S. Yamashita, N. Akasaka, S. Onose, S. Watanabe, H. Takahashi, J. Nucl. Sci. Technol. 44 (2007) 1535.
[282] T. Yamamoto, H. Kishimoto, G.R. Odette.reportFusion Materials Semiannual Report 7/1 to 12/31/2003 DOE/ER-313/34.
[283] E. Gaganidze, H.-C. Schneider, C. Petersen, J. Aktaa, A. Povstyanko, V. Prokhorov, R. Lindau, E. Materna-Morris, A. Möslang, E. Diegele, R. Lässer, B. van der Schaaf, E. Lucon, in: Proceedings of 22nd IAEA Fusion Energy Conference, October 13-18, 2008, Geneva, Switzerland, FT/P2-1.
[284] R. Chaouadi, J. Nucl. Mater. 372 (2006) 379.
[285] A.F. Rowcliff, J.P. Robertson, R.L. Klueh, K. Shiba, D.J. Alexander, M.L. Grossbeck, S. Jitsukawa, J. Nucl. Mater. 258–263 (1998) 1275.
[286] E. Gaganidze, C. Petersen, Post Irradiation Examination of RAFM Steels after Fast Reactor Irradiation up to 71 Dpa and <340 °C (ARBOR 2), EFDA TW5-TTMS-001 D10, Karlsruhe Institute of Technology, 2011. KIT Scientific Report 7596.
[287] E. Lucon, W. Vandermeulen, J. Nucl. Mater. 386–388 (2009) 254.
[288] F.A. Garner, M.B. Toloczko, B.H. Sencer, J. Nucl. Mater. 276 (2000) 123.
[289] D.S. Gelles, J. Nucl. Mater. 122–123 (1984) 207.
[290] M. Toloczko, F.A. Garner, C.R. Eiholzer, J. Nucl. Mater. 212–215 (1994) 604.
[291] J.M. Vitek, R.L. Klueh, J. Nucl. Mater. 122–123 (1984) 254.
[292] J. Van den Bosch, O. Anderoglu, R. Dickerson, M. Hartl, P. Dickerson, J.A. Aguiar, P. Hosemann, M.B. Toloczko, S.A. Maloy, J. Nucl. Mater. 440 (2013) 91.
[293] Y. Miwa, E. Wakai, K. Shiba, N. Hashimoto, J.P. Robertson, A.F. Rowcliff, A. Hishinuma, J. Nucl. Mater. 283–287 (2000) 334.
[294] Y. Kohno, D.S. Gelles, A. Kohyama, M. Tamura, A. Hishinuma, "Irradiation response of a reduced activation Fe-8Cr-2W martensitic steel (F82H) after FFTF irradiation," J. Nucl. Mater., Vols. 191–194, pp. 868-873.
[295] E. Wakai, N. Hashimoto, Y. Miwa, J.P. Robertson, R.L. Klueh, K. Shiba, S. Jitsukawa, J. Nucl. Mater. 283–287 (2000) 799.
[296] G.R. Odette, D. Frey, J. Nucl. Mater. 85–86 (1979) 817.
[297] R.L. Klueh, Phil. Mag. 98 (2018) 28, 2618.
[298] X. Wang, Q. Yan, G.S. Was, L. Wang, Scripta Mater. 112 (2016) 9.
[299] S. Hiwatashi, Y. Kohno, K. Asakura, A. Kohyama, J. Nucl. Mater. 179–181 (1991) 709.
[300] H. Ogiwara, H. Sakasegawa, H. Tanigawa, M. Ando, Y. Katoh, A. Kohyama, J. Nucl. Mater. 307–311 (2002) 299.
[301] E. Wakai, M. Ando, T. Sawai, K. Kikuchi, K. Furuya, M. Sato, K. Oka, S. Ohnuki, H. Tomita, T. Tomita, Y. Kato, F. Takada, J. Nucl. Mater. 356 (2006) 95.
[302] G. Was, Z. Jiao, E. Getto, K. Sun, A. Monterrosa, S. Maloy, O. Anderoglu, B. Sencer, M. Hackett, Scripta Mater. 88 (2014) 33.
[303] D. Brimbal, L. Beck, O. Troeber, E. Gaganidze, P. Trocellier, J. Aktaa, R. Lindau, J. Nucl. Mater. 465 (2015) 236.
[304] B. Kaiser, C. Dethloff, E. Gaganidze, D. Brimbal, M. Payet, P. Trocellier, L. Beck, J. Aktaa, J. Nucl. Mater. 484 (2017) 59.
[305] B. Kaiser, E. Gaganidze, C. Dethloff, R. Schwaiger, D. Brimbal, M. Payet, L. Beck, J. Aktaa, Nuclear Materials and Energy 15 (2018) 148.
[306] I. Sacksteder, H.-C. Schneider, E. Materna-Morris, J. Nucl. Mater. 417 (2011) 127.
[307] A. Uehira, S. Mizuta, S. Ukai, R. Puigh, J. Nucl. Mater. 283–287 (2000) 396.
[308] N.V. Luzginova, M. Jong, J.W. Rensman, J.B.J. Hegeman, J.G. van der Laan, J. Nucl. Mater. 417 (2011) 104.
[309] A. Kohyama, Y. Kohno, K. Asakura, M. Yoshino, C. Namba, C.R. Eiholzer, J. Nucl. Mater. 212–215 (1994) 751.
[310] M. Ando, M. Li, H. Tanigawa, M.L. Grossbeck, S. Kim, T. Sawai, K. Shiba, Y. Kohno, A. Kohyama, J. Nucl. Mater. 367–370 (2007) 122.
[311] M. Ando, T. Nozawa, T. Hirose, H. Tanigawa, E. Wakai, R.E. Stoller, J. Myers, Fusion Sci. Technol. 68 (2015) 648.
[312] M.R. Gilbert, S.L. Dudarev, S. Zheng, L.W. Packer, J.-Ch Sublet, Nucl. Fusion 52 (2012), 083019.
[313] R.L. Klueh, D.S. Gelles, S. Jitsukawa, A. Kimura, G.R. Odette, B. van der Schaaf, M. Victoria, J. Nucl. Mater. 307–311 (2002) 455.
[314] E. Gaganidze, J. Aktaa, Fus. eng. Design 83 (2008) 1498.
[315] E. Gaganidze, C. Petersen, J. Aktaa, J. Nucl. Mater. 386–388 (2009) 349.
[316] E. Wakai, N. Okubo, M. Ando, T. Yamamoto, F. Takada, J. Nucl. Mater. 398 (2010) 64.
[317] Y. Dai, W. Wagner, J. Nucl. Mater. 389 (2009) 288.
[318] Y. Dai, J. Henry, Z. Tong, X. Averty, J. Malaplate, B. Long, J. Nucl. Mater. 415 (2011) 306.
[319] R. Lindau, A. Möslang, D. Preininger, M. Rieth, H.D. Röhrig, J. Nucl. Mater. 271–272 (1999) 450.
[320] M. Klimenkov, A. Möslang, E. Materna-Morris, J. Nucl. Mater. 453 (2014) 54.
[321] R. Coppola, M. Klimenkov, A. Möslang, R. Lindau, M. Rieth, M. Valli, Nuclear Materials and Energy 17 (2018) 40.
[322] T. Yamamoto, G.R. Odette, P. Miao, D.J. Edwards, R.J. Kurtz, J. Nucl. Mater. 386–388 (2009) 338.
[323] H.U. Borgstedt, C.K. Mathews, in: Applied Chemistry of the Alkali Metals, Plenum Press, New York, 1987.
[324] E. Yoshida, T. Furukawa, in: D. Féron (Ed.), Nuclear Corrosion Science and Engineering, Woodhead Publishing Limited, Cambridge, UK, 2012 (Chapter 21).
[325] C. Fazio, F. Balbaud, in: P. Yvon (Ed.), Structural Materials for Generation IV Nuclear Reactors, Woodhead Publishing, Duxford, UK, 2017, p. 23.
[326] B. Barkia, T. Auger, J.L. Courouau, J. Bourgon, J. Mater. Res. 33 (2018) 121.
[327] J.L. Courouau, M. Tabarant, F. Rouillard, S. Tricoit, F. Balbaud-Célérier, V. Lorentz, C. Cabet, in: Proceedings of the International Workshop on Structural Materials for Innovative Nuclear Systems, Idaho Falls, ID, USA, 2013.
[328] J.L. Courouau, M.C. Steil, J. Fouletier, F. Rouillard, et al., Oxid. Metals 87 (2017) 789.
[329] J.R. Weeks, H.S. Isaacs, in: M.G. Fontana, R.W. Staehle (Eds.), Advances in Corrosion Science and Technology, Springer, Boston, MA, USA, 1973.
[330] M. Rivollier, J.L. Courouau, M. Tabarant, C. Blanc, M.L. Giorgi, J. Nucl. Mater. 500 (2018) 337.
[331] J.L. Courouau, V. Lorentz, M. Tabarant, S. Bosonnet, F. Balbaud-Célérier, in: Proceedings of the International Conference on Fast Reactors and Related Fuel Cycles: Safe Technologies and Sustainable Scenarios, Paris, France, 2013.
[332] A.W. Thorley, C. Tyzack, in: Proceeding of the International Conference Organized by the British Nuclear Energy Society, Nottingham University, London, 1973, p. 257.
[333] T. Gnanasekaran, R.K. Dayal, in: D. Féron (Ed.), Nuclear Corrosion Science and Engineering, Woodhead Publishing Limited, Cambridge, UK, 2012 (Chapter 10).
[334] T. Ito, S. Kato, M. Aoki, et al., J. Nucl. Sci. Technol. 29 (1992) 367.
[335] J.P. Hilditch, J.R. Hurley, P. Skeldon, D.R. Tice, Corros. Sci. 37 (1995) 445.
[336] S. Hémery, T. Auger, J.L. Courouau, F. Balbaud-Célérier, Corros. Sci. 76 (2013) 441.
[337] F. Balbaud-Célérier, L. Martinelli, in: D. Féron (Ed.), Nuclear Corrosion Science and Engineering, Woodhead Publishing Limited, Cambridge, UK, 2012 (Chapter 22).
[338] L. Martinelli, F. Balbaud-Célérier, Mater. Corros. 62 (2011) 531.
[339] B. Long, Y. Dai, N. Baluc, J. Nucl. Mater. 431 (2012) 85.
[340] I. Serre, J.B. Vogt, J. Nucl. Mater. 376 (2008) 330.
[341] L. Martinelli, T. Dufrenoy, K. Jaakou, A. Rusanov, F. Balbaud-Célérier, J. Nucl. Mater. 376 (2008) 282.
[342] O. Yeliseyeva, V. Tsisar, G. Benamati, C. Fazio, Corros. Sci. 50 (2008) 1672.
[343] A. Weisenburger, G. Müller, A. Heinzel, A. Jianu, et al., Nucl. Eng. Des. 241 (2011) 1329.
[344] I.G. Wright, R.B. Dooley, Int. Mater. Rev. 55 (2010) 129.
[345] P. Billard, R. Fillon, J. Gabrel, B. Vandenberghe, in: Proceedings of the 5th International Conference on Advances in Materials Technology for Fossil Power Plants, EPRI, 2008.
[346] L. Martinelli, C. Desgranges, F. Rouillard, K. Ginestar, et al., Corros. Sci. 100 (2015) 253.
[347] S. Teyssere, in: D. Féron (Ed.), Nuclear Corrosion Science and Engineering, Woodhead Publishing Limited, Cambridge, UK, 2012 (Chapter 24).
[348] Y. Chen, K. Sridharan, S. Ukai, T.R. Allen, J. Nucl. Mater. 371 (2007) 118.
[349] P. Ampornrat, G. Gupta, G.S. Was, J. Nucl. Mater. 395 (2009) 30.
[350] G. Gupta, P. Ampornrat, X. Ren, K. Sridharan, T.R. Allen, G.S. Was, J. Nucl. Mater. 361 (2007) 160.
[351] C. Cabet, F. Rouillard, J. Nucl. Mater. 392 (2009) 235.
[352] L.W. Graham, J. Nucl. Mater. 171 (1990) 76.
[353] F. Rouillard, T. Furukawa, Corros. Sci. 105 (2016) 120.
[354] S. Bouhieda, F. Rouillard, K. Wolski, Mater. A. T. High. Temp. 29 (2011) 151–158.

J. Henry graduated from the French University of Technology Ecole Centrale Paris and received a PhD in Materials Science from Paris Orsay University. After 3 years at the main research laboratory of the steelmaker Usinor-Sacilor (now Arcelor-Mittal), he joined the French Atomic Energy Commission (CEA). He is currently senior expert, head of the Materials Microstructural Analysis Laboratory within the Nuclear Materials Department (CEA Saclay) and leader of a EUROfusion Materials sub-project. His research interests include irradiation effects in fission/fusion/spallation environments on the microstructure and mechanical properties of structural and cladding materials.